

1 Advances in the Analysis of Biogeochemical Interfaces: NanoSIMS to
2 Investigate Soil Microenvironments

3 Review article for “Advances in Agronomy”

4 Carsten W. Mueller¹, Peter K. Weber², Matt R. Kilburn³, Carmen Hoeschen¹, Markus Kleber⁴
5 and Jennifer Pett-Ridge²

6 ¹Lehrstuhl für Bodenkunde, TU München, Freising, Germany

7 ²Chemical Sciences Division, Lawrence Livermore National Laboratory, Livermore,
8 California, USA

9 ³Centre for Microscopy, Characterisation and Analysis, The University of Western Australia,
10 Crawley, Australia

11 ⁴Department of Crop and Soil Science, Oregon State University, Corvallis, USA

12

13 Running head: NanoSIMS to Investigate Soil Microenvironments

14 Corresponding author: Carsten W. Mueller, carsten.mueller@wzw.tum.de,

15 phone: +49(0)8161-714423, FAX: +49(0)8161-714466

16 Used platform: Windows XP, Word 2010

17 Date: 11. October 2012

18

19	Table of Contents
20	Abstract
21	1. Introduction
22	1.1. The importance of nano-scale processes in soils research
23	1.2. Fundamentals of Secondary Ion Mass Spectrometry
24	1.2.1 NanoSIMS
25	1.2.2. Basic requirements for NanoSIMS samples
26	2. Experimental approaches for the study of soil microenvironments using NanoSIMS
27	2.1. Lessons learned from geology and microbiology
28	2.1.1. Investigating mineral-organic associations
29	2.1.2. Investigating intact three dimensional micro-structures
30	2.1.3. Investigating plant – soil processes
31	2.1.4. Tracking organic and inorganic pollutants
32	3. NanoSIMS requirements for soil related studies
33	3.1. Technical considerations for soil samples
34	3.2. Sample documentation
35	3.3. Instrument tuning and quality control
36	3.4. Sample preparation – from single particles to intact soil
37	3.4.1. Direct deposition of individual particles and microaggregates
38	3.4.2. Fixation and preparation of organic materials
39	3.4.3. Preparation of aggregated soil structure and intact plant-soil systems
40	3.5. Data acquisition and analysis
41	4. Combination with other micro-scale techniques

42	4.1.	Scanning and transmission electron microscopy
43	4.2.	Synchrotron based techniques
44	4.3.	Atomic force microscopy
45	4.4.	In situ single-cell labeling
46	5.	Conclusion
47		Acknowledgments
48		References
49		

50 **Abstract**

51 Since a NanoSIMS high-resolution secondary ion mass spectrometry instrument was first
52 used for cosmochemistry investigations over a decade ago, both interest in NanoSIMS and
53 the number of instruments available have significantly increased. However, SIMS comes with
54 a set of challenges that are of both technical and conceptual nature, particularly for complex
55 samples such as soils. Here, we synthesize existing research and provide conceptual and
56 technical guidance to those who wish to investigate soil processes at the sub-micron scale
57 using secondary ion mass spectrometry, specifically with NanoSIMS. Our review offers
58 advice resulting from our own operational experience but also intends to promote synergistic
59 research on yet unresolved methodological issues. We identify and describe the basic setup
60 of a NanoSIMS instrument and important issues that may arise as a soil sample specimen is
61 prepared for NanoSIMS analysis. This is complemented by discussions of experimental
62 design, data analysis and data representation. Next to experimental design, sample
63 preparation is the most crucial prerequisite for successful NanoSIMS analyses. We discuss
64 the requirements and limitations for sample preparation over the size range from individual
65 soil particles to intact soil structures such as macroaggregates or intact soil cores. For robust
66 interpretation of data obtained by NanoSIMS, parallel spatial, textural (scanning electron
67 microscopy, atomic force microscopy) or compositional analyses (scanning transmission X-
68 ray microscopy) are often necessary to provide necessary context. We suggest that
69 NanoSIMS analysis is most valuable when applied in concert with other analytical
70 procedures and can provide powerful inference about small scale processes that can be
71 traced via isotopic labeling or elemental mapping.

72

73 1. Introduction

74 1.1. The importance of nano-scale processes in soils research

75 Soil is often described as one of the most complex media on earth (Schulze and Freibauer,
76 2005). This complexity extends from the ecosystem-scale to individual microaggregates,
77 where nanometer-scale interactions between microbiota, organic matter and mineral
78 particles are thought to control the long-term fate of soil carbon, nutrients and pollutants
79 (Lehmann et al., 2007; Schmidt et al., 2011). Processes that have a major impact at the
80 landscape- or global-scale are determined by events occurring at the micro- and nanometer
81 scales. For example, entrapment of soil organic matter (SOM) within microaggregates with a
82 diameter of less than 250 μm and SOM sorption onto even smaller clay and iron oxides is a
83 vital mechanism for long term preservation of organic carbon (OC) in soils (Lehmann et al.,
84 2007; von Lützow et al., 2006). Release of nutrients in the rhizosphere is driven by root
85 exudation at highly active micron-scale biogeochemical interfaces between roots, microbes
86 and minerals (Breland and Bakken, 1991; Hinsinger et al., 2009; Norton and Firestone,
87 1996). Microbial activity occurs mostly in micro-habitats (Dechesne et al., 2007; Müller and
88 Defago, 2006; Nunan et al., 2007) and involves mineralization of SOM and organic
89 pollutants. Hydrologic processes at the field-scale are also influenced by fine-scale
90 interactions as preferential flow paths may create localized zones of altered water and
91 nutrient flow and thereby impact microbial abundance, community structure and SOM
92 turnover (Chabbi et al., 2009; Morales et al., 2010). Preferential flow zones are themselves
93 heterogeneous at the micro-scale, with a heterogeneous supply of oxygen, water and
94 nutrients driving “hot spots” of microbial growth directly adjacent to areas of lesser microbial
95 activity (Bundt et al., 2001). In all of these cases, activities at nano- to micron-scale soil
96 biogeochemical interfaces determine the expression of higher level ecosystem functions. The
97 majority of soil research, however, is conducted on bulk ($> 1 \text{ g}$) samples, which are often
98 significantly altered prior to analysis. Pretreatments and analytical side effects include drying
99 at varying temperatures, sieving/homogenization for process or elemental analysis, thermal
100 alteration (as in pyrolysis GC/MS) or chemical alteration (as in alkaline extraction of “humic”

101 substances or in cupric oxide oxidation for lignin analyses). With the advent of novel micro-
102 spectroscopy and spectrometry techniques that allow for the study of micro- to nano-scale
103 molecular, isotopic, and elemental patterns, it is now possible to make process-oriented
104 observations (e.g. the stabilization of organic matter, sorption of pollutants and mineral
105 weathering) at the micron or sub-micron scale.

106 Elemental and isotopic imaging conducted via secondary ion mass spectrometry (SIMS) is a
107 particularly promising technique for small-scale soil process research. SIMS uses a high-
108 energy ion beam to sputter material from a sample surface, which can then be analyzed in a
109 mass-spectrometer. With high resolution SIMS instruments (Cameca NanoSIMS 50, 50L,
110 Gennevilliers, France), the distribution of elements and isotopes can be visualized with up to
111 50-150 nm lateral resolution within soil samples ranging from primary particles to sub-regions
112 of intact soil cores. For this reason, NanoSIMS has the potential to provide quantitative
113 measures of organic matter-mineral-microbial interactions and biogeochemical processing at
114 the macro- and microaggregate or single-cell scale.

115 Relatively few SIMS experiments have been conducted to date in soil science. In one of the
116 first, Cliff *et al.*, (2002b) used time of flight-SIMS (ToF-SIMS) and additions of ¹⁵N-labeled
117 and ¹³C-labeled compounds to study small-scale differences in N assimilation as a function of
118 C vs. N limitation. When they compared SIMS values with bulk-measured microbial biomass
119 N assimilation, they found substantial spatial heterogeneity in ¹⁵N distribution that was not
120 apparent through bulk analysis (Cliff *et al.*, 2007). More recently, studies using SIMS and
121 NanoSIMS analysis have revealed effects at even finer scales within individual
122 microaggregates, mineral surfaces, microbes, and root hairs (Blair *et al.*, 2006; Cliff *et al.*,
123 2002a; Clode *et al.*, 2009; DeRito *et al.*, 2005; Herrmann *et al.*, 2007a; Herrmann *et al.*,
124 2007b; Keiluweit *et al.*, 2012; Pumphrey *et al.*, 2009). An early review paper by Herrmann
125 and co-authors (Herrmann *et al.*, 2007b) focused on potential applications for soil ecology
126 and included the first application of the NanoSIMS technique with an intact soil
127 microaggregate. Subsequent publications have addressed the technical aspects (sample

128 preparation) and investigations of organo-mineral associations at scales ranging from clay
129 size mineral grain to intact soil cores (Keiluweit et al., 2012; Mueller et al., 2012b; Remusat
130 et al., 2012).

131 In this article, our goal is to provide insight into the range of potential NanoSIMS applications
132 in soil system research, discussing technical capabilities and limitations, major sample
133 requirements, and important complementary micro-spectrometry techniques. As NanoSIMS
134 applications in closely related fields, such as plant science and microbiology, have been
135 reviewed recently (Moore et al., 2011a; Musat et al., 2012), we focus on the use of
136 NanoSIMS in soil research.

137 1.2. Fundamentals of Secondary Ion Mass Spectrometry

138 SIMS is a surface analysis technique for solid samples. Primary ions, with a kinetic energy
139 ranging from a few hundred electron volts to tens of thousands of electron volts, are focused
140 on the sample surface, ejecting atoms and molecules in a process called sputtering (see
141 Figure 1). A small fraction of the ejected atoms and molecules are ionized, and can be
142 extracted with an electrostatic field into a mass spectrometer. The fraction of the sputtered
143 material that is ionized is determined by the ionization efficiency of the element in the sample
144 matrix, and is referred to as the secondary ion yield. For different elements, secondary ion
145 yields vary over many orders of magnitude, and also strongly depend on the physico-
146 chemical nature of the sample (Storms et al., 1977; Wilson et al., 1989). Within the mass
147 spectrometer, secondary ions can be separated according to their mass to charge ratio in a
148 quadrupole, magnetic-sector, or time-of-flight (TOF) mass analyzer. These analyzers differ in
149 terms of detectable mass range, sensitivity, ion transmission, and cost. As NanoSIMS has
150 both high sensitivity and spatial resolution at high mass resolving power, this particular SIMS
151 instrument meets many of the specific requirements for micro-scale elemental and isotopic
152 mapping analyses in soil science.

153

154 1.2.1. NanoSIMS

155 The NanoSIMS is optimized for SIMS imaging with sub-micron lateral resolution. The
156 NanoSIMS 50 and 50L instruments, conceived by George Slodzian (Slodzian, 1987;
157 Slodzian et al., 1992) was designed by Bernard Daigne, François Girard and François Hillion
158 (Hillion et al., 1993), and manufactured by Cameca France under a license from the Office
159 National d'Études et de Recherches Aérospatiales at Université Paris-Sud (UPS ONERA).
160 There are now more than thirty NanoSIMS instruments installed world-wide, working on a
161 wide range of applications ranging from geology and cosmochemistry (Floss et al., 2006;
162 Hoppe, 2006; Stadermann et al., 1999; Wacey et al., 2010a), to biology (Finzi-Hart et al.,
163 2009; Kraft et al., 2006; Lechene et al., 2006), material science (Valle et al., 2011) and soil
164 science (Herrmann et al., 2007a; Keiluweit et al., 2012; Mueller et al., 2012b).

165 The key innovation of the NanoSIMS is the coaxial lens (Figure 1) which focuses the primary
166 ion beam and extracts and focuses the secondary ion beam as well. This configuration
167 minimizes the distance between the sample surface and primary focusing lens, allowing the
168 primary beam to be focused to a much smaller diameter than in conventional SIMS
169 instruments. In addition, the secondary mass spectrometer is optimized for high-transmission
170 at high (>3000) mass resolving power. The NanoSIMS comes equipped with a Cs⁺ primary
171 ion source for analysis of negative secondary ion species (e.g. ¹²C⁻, ¹³C⁻, ¹²C¹⁴N⁻, ¹²C¹⁵N⁻,
172 ²⁸Si⁻, ²⁷Al¹⁶O⁻ and ⁵⁶Fe¹⁶O⁻), and an O⁻ primary beam source, for analysis of positive
173 secondary ions (e.g. ²³Na⁺, ³⁹K⁺, ⁴⁴Ca⁺, ⁵⁶Fe). Due to the coaxial lens setup (Figure 1 B),
174 secondary ions must have the opposite charge from primary ions to enable extraction to the
175 mass spectrometer. A ~150 nm diameter Cs⁺ primary ion beam with a beam current of 1 to 2
176 pico Ampere can routinely be achieved. While an even smaller beam diameter is possible,
177 there are trade-offs between high-resolution (with reduced beam current) and secondary ion
178 count rates. Higher currents and thus beam diameters are often crucial to yield significant
179 amounts of secondary ions (e.g. ¹³C⁻, ¹²C¹⁵N⁻, ⁵⁶Fe¹⁶O⁻) when analyzing soil samples. With an
180 O⁻ beam, a diameter of ~400 nm is typical.

181 The advantage of the NanoSIMS instrument lies in the coupling of a continuous, high spatial
182 resolution analysis beam with high mass resolving power, resulting in high sensitivity and
183 specificity with relatively short integration times. Users should also be fully aware that the
184 NanoSIMS 50 and 50L are both 'dynamic' SIMS instruments where the sample is actively
185 eroded during the sputtering process and molecular bonds are broken by the primary ion
186 beam. Up to five (NanoSIMS 50) or seven (NanoSIMS 50L) secondary ions can be detected
187 simultaneously. Additionally, if operated in Cs⁺ mode, secondary electrons produced by the
188 collision cascade can be detected by a photo-multiplier, providing a secondary electron
189 image that can provide structural and textural information that is comparable to a low-
190 resolution SEM micrograph.

191 1.2.2. Basic requirements for NanoSIMS samples

192 A wide range of solid samples are compatible with SIMS, provided they are dry and stable
193 under high vacuum (< 10⁻⁹ mbar), relatively flat (< 2-30 microns of relief), and conductive.
194 Sample out-gassing can be caused by absorbed water, other volatiles, hydrocarbons or
195 samples prepared via resin embedding. Pre-treatment in a vacuum oven under low heat can
196 reduce out-gassing within the analysis chamber. Out-gassing may degrade analysis
197 conditions by elevating chamber pressure, reducing ion transmission and generating
198 molecular interferences or physical contamination, which will all lead to poor analysis quality.
199 Sample flatness is also important as any surface roughness may influence sample
200 sputtering, ion extraction and mass spectrometer tuning. For natural abundance isotopic ratio
201 measurements, 2-4 per mil level external precision can be achieved with repeated analyses
202 of bacterial spores with ~1 micron of relief (P.K. Weber, unpublished results). For isotopic
203 tracer experiments, more topographic relief (10 to 20 microns) can be tolerated (Woebken et
204 al., 2012). Even higher topographic relief (~30 microns) may also be viable in some
205 applications (P.K. Weber, unpublished results) but with significant loss in precision and the
206 need for careful monitoring of measurement quality. Finally, because SIMS uses an ion
207 beam to eject charged ions from the sample's upper atomic layers, a mechanism to dissipate

208 charge from the analysis location is critical. In our experience, most soil samples are semi-
209 insulating, and typically must be coated in an evaporator or sputter coater with a 2 – 20 nm
210 layer of gold (or carbon, iridium, gold-palladium, or platinum) to minimize charging during
211 analysis. Sample flatness can also interact with charge dissipation characteristics. As a
212 general rule, the more topography a sample has, the thicker a conductive coat needs to be to
213 bridge topographic gaps. Metal coating and sample flatness become particularly important if
214 an electron flood gun is to be used for charge compensation (see NanoSIMS soil preparation
215 details below).

216 **2. Experimental approaches for the study of soil microenvironments using** 217 **NanoSIMS**

218 2.1. Lessons learned from geology and microbiology

219 Perhaps one of the most appealing aspects of NanoSIMS analysis for many soil scientists is
220 the instrument's potential to quantitatively localize stable isotopes at a previously unresolved
221 spatial scale. Since the fields of geology, cosmochemistry, and geomicrobiology have a more
222 extensive tradition with SIMS and NanoSIMS applications, that literature is a logical source of
223 illustrative models for soils research. Cosmochemists were first to use NanoSIMS for isotopic
224 measurements, taking advantage of its high spatial resolution and simultaneous imaging
225 capabilities. Using NanoSIMS, Messenger et al. (2003) located rare isotopically anomalous
226 (> 100 ‰) micron-sized pre-solar grains within meteoritic samples that are too small to have
227 been analyzed by bulk measurements or even conventional SIMS (e.g. Cameca SIMS 1280).
228 NanoSIMS has also been used to measure large isotopic fractionation in biominerals (e.g.
229 carbonates from mollusk shells and corals) and deduce metabolic pathways such as
230 methanotrophy (Rasmussen et al., 2009) or sulfate reduction and sulfur disproportionation
231 (Philippot et al., 2007; Wacey et al., 2010b). In geologic samples, NanoSIMS imaging was
232 employed to support a microbial origin for Ooids - concentrically-laminated sedimentary
233 grains found in turbulent marine and freshwater environments (Pacton et al., 2012), and a

234 microbial role in Fe-mineralization within spheroidal iron oxide concretions associated with
235 palaeoaquifers (Weber et al., 2012).

236 All of the studies mentioned above capitalized upon natural isotope fractionation effects that
237 can shift natural abundance values by 10s to 100 per mil (e.g. for biological sulfur cycling -
238 8.5‰ to +19‰ $\delta^{34}\text{S}_{\text{CDT}}$ (CDT – Canyon Diablo troilite); for methanotrophy -55‰ to -43‰
239 $\delta^{13}\text{C}_{\text{PDB}}$ (PDB – Pee Dee belemnite) (Rasmussen et al., 2009). These effects are in many
240 cases significantly larger than those found in soil/sediment systems, where prominent
241 isotopic effects range from ~ 1 to 11‰ $\delta^{13}\text{C}$ (litter decomposition, C3-C4 plant shifts,
242 (Ehleringer et al., 2000)), ~7‰ $\delta^{15}\text{N}$ (soil depth gradients, (Billings and Richter, 2006)) or as
243 little as 0.8‰ $\delta^{56}\text{Fe}$ (soil iron pools, (Kiczka et al., 2011)). One exception is the work of
244 Orphan and colleagues (2001) who have used SIMS and NanoSIMS to image isotopic
245 fractionation in modern anoxic sediment cores of the Eel river basin in the Pacific Ocean.
246 There, the authors report isotopic fractionations of $\delta^{13}\text{C}$ of up to -96‰ in the interior of
247 bacterial aggregates, indicating consumption of isotopically light methane by methanotrophic
248 bacteria.

249 For most soil process-level questions, the best approach may be to use stable isotope
250 labeling as a way to document transformation pathways in soil micro-environments over time.
251 This approach, like many of the published examples in cosmo- and geo-chemistry, would
252 take full advantage of the NanoSIMS's spatial resolution while improving detection of the
253 isotopic species of interest. In the past decade, stable isotope labeling (often with ^{13}C or ^{15}N)
254 and NanoSIMS analyses have been widely used in environmental microbiology, supporting
255 research on the metabolism of single microbial cells (Pett-Ridge and Weber, 2012) both in
256 pure culture and in natural environmental samples ranging from marine bacterial and
257 archaeal communities (Dekas et al., 2009; Halm et al., 2009; Musat et al., 2008; Ploug et al.,
258 2010), to acid mine drainage biofilms (Moreau et al., 2007), to ^{13}C and ^{15}N fixation in
259 diazotrophic cyanobacteria (Finzi-Hart et al., 2009; Popa et al., 2007; Woebken et al., 2012)
260 and eukaryotes (Lechene et al., 2006; Lechene et al., 2007).

261 An idealized stable isotope labeling experiment in soil might proceed as follows: (1) add an
262 organic compound of interest, labeled for instance with ^{13}C or ^{15}N , to a model system that
263 contains reactive mineral surfaces and an active microbial decomposer community; (2)
264 incubate under controlled conditions, varying an edaphic variable of interest (moisture,
265 temperature, pH); (3) prepare and analyze samples via NanoSIMS imaging to determine the
266 physical fate of the target compound – whether it becomes metabolized (and the label is
267 transferred to microbial decomposers) or whether it is adsorbed to mineral surfaces.
268 Enrichment of the label above a background value could then be used to support inference
269 about the fate of the compound of interest. This type of application could potentially
270 contribute to both studies of soil carbon turnover dynamics as well as investigations of
271 contaminant fate in soils.

272 Previous NanoSIMS studies of biotic (microorganisms and plants) and abiotic materials
273 (minerals, fossils) represent endmember models of the soil system, with its inherent
274 combination of geologic and microbiological aspects. This substantial literature serves as a
275 valuable resource for soil scientists interested in designing micro-scale soil research,
276 particularly as a resource for experimental concepts and sample preparation protocols. In the
277 following section we discuss examples from soil science where NanoSIMS has been
278 successfully applied, as well as additional areas where soil interface research could
279 significantly benefit from high-resolution isotopic imaging in the future. As we point out
280 potential applications, we also mention pitfalls and methodological constraints.

281 2.1.1 Investigating mineral-organic associations

282 Historically, studies of mineral-organic associations have employed bulk analysis procedures
283 performed on operationally defined physical fractions (Balesdent et al., 2000; Christensen,
284 2001; Eusterhues et al., 2005; Schöning et al., 2005). The goal of such procedures is to
285 isolate mineral-organic associations of given characteristics, such as an increasing
286 proportion of microbially processed organic matter (OM) in fractions of increasing density
287 (Derrien et al., 2006; Grandy and Neff, 2008; von Lützow et al., 2007). In contrast to bulk

288 analysis, NanoSIMS offers the possibility to examine organo-mineral assemblages in the
289 context of intact spatial structures. If a stable isotope labeling experiment (see above) is
290 used, NanoSIMS images can potentially reveal the spatial distribution and dilution of a tracer
291 material as it moves into the soil matrix. They can also reveal whether preferential
292 associations of certain OM types predictably associate with certain mineral phases. This is
293 possible because of three main advantages NanoSIMS has over other microscopic
294 techniques: (1) elemental mapping can be done with better lateral resolution, (2) the low
295 depth penetration (~ 10 to 20 nm) of the NanoSIMS primary beam allows thin surface layers
296 to be examined, (3) highly accurate isotope detection allows the operator to track OM¹³C and
297 OM¹⁵N onto distinct minerals in an intact micro-environment, and thus enables process-level
298 studies. In a proof-of concept example, these three advantages were exploited by Heister et
299 al. (2012), who showed that in artificial soil mixtures, soil minerals and organic materials can
300 be distinguished in NanoSIMS images, using the distinction between organic material
301 derived ions (¹²C⁻ and ¹²C¹⁴N⁻) and mineral derived ions (²⁸Si⁻, ²⁷Al¹⁶O⁻, and ⁵⁶Fe¹⁶O⁻). The
302 authors used NanoSIMS in this study as a tool for micro-scale elemental mapping of organic
303 matter on mineral surfaces. They showed that organic matter tended to be attached to
304 phyllosilicate clays in the form of isolated patches, while continuous coatings of organic
305 matter enveloped small ferrihydrite particles. Such micro-scale heterogeneities could not
306 have been resolved by SEM/EDX measurements. In another example, Mueller et al. (2012b),
307 working with resin-embedded soil macroaggregates, found heterogeneous isotopic
308 enrichment at the micro-scale following the application of a ¹³C/¹⁵N label (amino acid mixture
309 of algal origin) to natural soils. They speculated that microbial activity may have lead to the
310 increased utilization of freshly added organic matter, or that soil components have different
311 sorption capacities. The NanoSIMS's unique capacity to detect stable isotope tracers at the
312 micro-scale enabled both these studies to confirm the predicted physical dimensions of
313 organo-mineral associations.

314 By combining isotopic and elemental imaging, NanoSIMS analysis can also reveal whether
315 certain OM types predictably associate with certain mineral phases. This particular capacity

316 of the NanoSIMS was used by Keiluweit et al (2012) in a study where $^{13}\text{C}/^{15}\text{N}$ enriched fungal
317 hyphal extracts were incubated with organic horizon soil. NanoSIMS images of ^{15}N
318 enrichment and iron distribution suggest that nitrogen from fungal cell walls was rapidly and
319 preferentially deposited as thin organic coatings onto Fe (hydr)oxide surfaces (Keiluweit et
320 al., 2012). Further analysis of these samples by scanning transmission X-ray microscope in
321 combination with near edge X-ray absorption fine structure spectrometry (STXM-NEXAFS)
322 revealed these soil microstructures were enriched in aliphatic C and amide N, suggesting
323 that a concentration of microbial lipids and proteins had quickly become associated with Fe
324 (hydr)oxide surfaces. Remusat et al. (2012) used a similar approach to image intact soil
325 particles with low levels of isotopic enrichment sampled 12 years after a ^{15}N litter labeling
326 experiment in a temperate forest. They describe microsites of isotopic enrichment (" ^{15}N hot
327 spots") on mineral surfaces, and in one microsite, suggest that ^{15}N enrichment was also
328 linked to the presence of microbial metabolites. This kind of combined approach, NanoSIMS
329 image analysis joined to complementary microscopy (SEM-EDX, STXM/NEXAFS), may be a
330 particularly profitable means to infer the molecular and spatial fate of labeled organic
331 materials in a mineral matrix, and has the potential to contribute to a mechanistic
332 understanding of sorption, occlusion, and decomposition processes that operate at fine
333 spatial scales.

334 A recent quantitative analysis of organo-mineral assemblages by Hatton et al. (2012) used a
335 combination of macro- and micro-scale analyses for an internal calibration of C/N and $^{15}\text{N}/^{14}\text{N}$
336 ratios in sequentially separated soil density fractions. This approach is based on the
337 assumption that macroscopic features, visible under reflectance light microscope and
338 analyzable by elemental analyzer isotope ratio mass spectrometry (EA-IRMS), are also
339 found at the micro-scale as detected in SEM or NanoSIMS images. The authors collected
340 NanoSIMS images over $500\ \mu\text{m}^2$ for each density SOM fraction, and corrected these using
341 EA-IRMS data from macroscopic features. Because matrix-matching SIMS standards for soil
342 organic matter do not yet exist, this calibration approach is a promising step towards a better
343 quantification of data derived from SIMS images. While significant procedural challenges

344 remain, the examples presented above illustrate how well-designed experiments can benefit
345 from NanoSIMS information to help decipher chemical and microbiological processes in soil
346 microenvironments.

347 2.1.2 Investigating intact three dimensional micro-structures

348 NanoSIMS imaging may also be profitable in studies of micro-scale soil architecture. The first
349 systematic approach to the study of in-situ soil features was established by the
350 micropedological work of Kubiena (1938). Whole intact soil clods were impregnated with
351 epoxy resin, thin sections were produced and small scale pedological features were studied
352 using transmitted light microscopy. A large range of soils have been studied using this
353 technique, combining different light sources ranging from polarized light to fluorescent
354 staining of microbial cells (Bullock and Murphy, 1980; Eickhorst and Tippkoetter, 2008; Fisk
355 et al., 1999; Li et al., 2004; Pulleman et al., 2005). With the rise of analytical techniques that
356 can resolve soil features at the nano- to micro-scale (e.g. TEM, AFM, NanoSIMS), the
357 micromorphological examination of soils is experiencing a renaissance. However, mineral
358 particles pose a challenge to elemental mapping and isotope tracing experiments in intact
359 soil matrices because they make embedding and thin-sectioning more difficult, and can
360 cause electrical charging effects (Cliff et al., 2002b; Pett-Ridge et al., 2012). Still, a number
361 of proof-of-concept studies have successfully shown that ^{15}N and ^{13}C isotope additions can
362 be imaged by NanoSIMS in two dimensions within a natural or synthetic soil matrix
363 (Herrmann et al., 2007b; Keiluweit et al., 2012; Mueller et al., 2012b; Pett-Ridge et al., 2012;
364 Remusat et al., 2012).

365 Sample preparation is the most important issue to be resolved prior to micro-scale studies of
366 soil three dimensional structures. This is particularly true for soil macroaggregates (> 250 μm
367 in diameter) which have topography too large for reliable NanoSIMS measurements. To
368 maintain adequate flatness and integrity in friable samples, larger soil aggregates and intact
369 soil cores will typically require embedding and subsequent sectioning. However, simply
370 cutting large aggregates into sections can affect structural integrity. One solution is thin

371 sectioning, although the approach used must be chosen with the target ions in mind. The
372 most important considerations include:

373 Does the sample contain both mineral and organic phases?

374 Might the embedding medium dilute the signal of the target species (e.g. ^{13}C)?

375 Is *in situ* hybridization to be used, and are diffusible ions or molecules of interest?

376 We discuss the finer details of these concerns in Sections 3.3.2 and 3.3.3. In general, our
377 experience has shown that for smaller macroaggregates (~250 μm) cryosectioning is a
378 laborious but worthwhile technique to obtain cross sections while avoiding contamination with
379 any artificial C or N sources. For examination of whole intact soil cores or macroaggregates
380 (several mm in diameter) resin embedding is currently the best option, although it introduces
381 an artificial C and N source, which can interfere with both isotopic analyses and techniques
382 to determine the chemical structure of OM (e.g. STXM). If target ions include C and N, resin
383 embedding should thus be used only for larger volume soil specimens consisting of a friable
384 porous network of organic and mineral particles that have to be tightly bound together in
385 order to allow cross sectioning and polishing. However, for some resins (e.g. Araldite 502)
386 the $^{12}\text{C}^{14}\text{N}/^{12}\text{C}$ ratio allows to distinguish between sample OM and embedding agent (Weber
387 et al., 2012). The resin embedding approach has been used to prepare slices of intact soil
388 cores for elemental mapping of in-situ interfaces in a buried Oa horizon originating from a
389 permafrost-affected soil in Northern Alaska (Typic Aquiturbel, coastal plain near Barrow)
390 (Figure 2). In this case, NanoSIMS imaging was used for elemental mapping of natural
391 micro-scale features at a scale which could not be resolved by comparable techniques such
392 as SEM-EDX. This example shows how NanoSIMS can illustrate the patterning of distinct
393 phases (organic matter ($^{12}\text{C}^{14}\text{N}$), organo-mineral interfaces, plant cells) via elemental
394 mapping of such friable and highly heterogeneous intact soil structures.

395 2.1.3 Investigating plant – soil processes

396 The interfaces between plant roots and soil (rhizosphere) or fungal hyphae and minerals
397 (hyphaesphere) are extremely biologically active and important sites for mineral weathering

398 (Finlay et al., 2009). Hinsinger et al. (2009) suggest that a lack of suitable observational tools
399 stands in the way of a better understanding of micro-scale elemental distributions in the
400 rhizosphere. Here NanoSIMS might well fill the gap between reflectance light microscopic
401 (e.g. epifluorescence, polarized light) and x-ray techniques (e.g. x-ray tomography) to trace
402 C, N and nutrient transfers between roots, microbes and soil. For the biotic side of the plant-
403 soil system, Gea et al. (1994) showed the utility of SIMS by imaging Ca in ectomycorrhizal
404 fungi (*Hebeloma cylindrosporum*) associated with pine trees (*Pinus pinaster*). Figure 3 is a
405 proof-of-concept of how NanoSIMS may be used to explore an intact plant-soil system at the
406 micro-scale. In this example, a French oak (*Quercus robur*) seedling was grown in a
407 vermiculite / soil mixture with a mycorrhizal fungi *Piloderma croceum* in order to track
408 interfaces between mineral constituents and the plant root. NanoSIMS images of an
409 embedded oak root tip illustrate that clay minerals may be distinguished from root cells and
410 mycorrhizal cells within the vermiculite layers, revealing the interfaces between the mineral
411 soil compartment, roots, and mycorrhizal fungi. This example demonstrates how NanoSIMS
412 images might contribute to the exploration of intact plant-soil-microbe interfaces.

413 Part of the difficulty associated with attempts to image the interfaces between plants,
414 microbes and mineral particles has to do with preparing samples in a manner that adequately
415 preserves these interfaces. A challenging but promising approach to preserve intact soil
416 architecture was demonstrated by Clode et al. (2009) who prepared 100 nm thick cross-
417 sections of ¹⁵N labeled wheat roots and associated bacteria by slowly infiltrating with araldite
418 epoxy over the course of several days. The resulting epoxy blocks were thin-sectioned and
419 then observed by both TEM and NanoSIMS at the University of Western Australia. The TEM
420 images clearly identified bacteria attached to the cortical cell walls, while NanoSIMS imaging
421 revealed that not all of the bacteria had incorporated the ¹⁵N label (Figure 4). While it is
422 possible that some cells were not metabolically active or dead, it is equally possible that
423 some of the ¹⁵N 'hotspots' were actually remnant effects of salts derived from the enriched
424 precursor material ((¹⁵NH₄)₂SO₄). This is a case where a complementary technique, for
425 example fluorescent in situ hybridization (FISH) or a live/dead or DAPI stain (see section

426 4.4.), might be useful to corroborate whether enriched features in NanoSIMS images truly
427 are bacterial cells.

428 2.1.4 Tracking organic and inorganic pollutants

429 Organic and inorganic pollutants span a wide range of molecular properties and may be
430 involved in a host of mechanistically different interactions with soil solids. Important inorganic
431 pollutants are metals and metalloids (e.g. Pb, As) (Bradl, 2004; Wilson et al., 2010; Zimmer
432 et al., 2011), including radioactive particles from nuclear accidents (Carbol et al., 2003;
433 Spezzano, 2005). Organic pollutants are inherently more diverse, encompassing the full
434 range from nonpolar polycyclic aromatic hydrocarbons to relatively polar chlorinated
435 hydrocarbons and polychlorinated biphenyls. To date, SIMS has been used to study the
436 micro-scale distribution of metals (e.g. Cd, Cr), metalloids (e.g. As), and halogens and
437 organic pollutants in microbial cells (Eybe et al., 2008), plants (Lombi et al., 2011;
438 Mangabeira et al., 2006; Martin et al., 2001; Migeon et al., 2009; Moore et al., 2010; Moore
439 et al., 2011b; Tartivel et al., 2012), animals (Eybe et al., 2009) and human tissues (Audinot et
440 al., 2004). NanoSIMS has been used to examine plutonium transport in the subsurface of
441 heavily contaminated sites (parts per million levels) (Kips et al., 2012; Novikov et al., 2006).
442 When there is substantial contamination, Pu can be directly imaged in situ and the
443 association of Pu with specific minerals can be determined to constrain transport
444 mechanisms. An intriguing example of a system comparable to primary soil particles (e.g.
445 clay minerals, OM particles) was presented by Krein et al. (2007), who located heavy metal
446 accumulation in aerosols using NanoSIMS by imaging $^{63}\text{Cu}^-$, $^{75}\text{As}^-$, $^{118}\text{Sn}^-$ and $^{123}\text{Sb}^-$. This
447 work suggests that it is possible to determine spatial dependencies between organic matter
448 and inorganic pollutants and evaluate 'hot spots' on micron-scale particles.

449 The primary limitations for NanoSIMS studies on organic pollutants are the vapor pressure of
450 the target pollutants (e.g. non-volatile organic compounds), the concentration of the target,
451 and incorporating a tracer for the target. Eybe et al. (2008) embedded *Anabaena* sp. cells
452 grown on the pesticide deltamethrin in an epoxy resin. To trace the pesticide within the

453 embedded cells, $^{81}\text{Br}^-$ was imaged in the NanoSIMS, illustrating how halogen containing
454 pollutants may be used as tracers within biological samples. Another example is the work of
455 Tartivel et al. (2012), who traced bromotoluene by the imaging of $^{81}\text{Br}^-$ in chemically fixed
456 plant roots (*Hedera helix*) and resin embedded soil cross sections.

457 3. NanoSIMS requirements for soil related studies

458 3.1. Technical considerations for soil samples

459 With its improved primary ion optics and secondary ion transmission at high mass resolving
460 power the NanoSIMS 50 and 50L enable SIMS analysis at the nanometer scale. However,
461 there are specific technical limitations that the potential user must consider, especially for
462 soils applications. While primary beams smaller than 50 nm are possible with idealized
463 samples, the number of ions collected from the impacted volume starts to fall below the
464 useful level in soils. NanoSIMS is a high vacuum ($\sim 10^{-10}$ Torr) instrument that requires
465 samples to be dehydrated, conductive and have low topography (ideally submicron for
466 natural abundance and < 30 micron-scale for isotopic enrichment experiments). As a result,
467 live microbial cells cannot be tracked, and to measure process effects over time, one must
468 rely on sub-sampling and replication. Samples should be fixed and can be thin-sectioned to
469 achieve a flat surface, ideally without re-arranging the locale of target elements or molecules.
470 While not currently available, a cryogenic stage might allow frozen samples to be analyzed,
471 thereby preserving them in a more natural state.

472 Though analyses of natural abundance ^{13}C and ^{15}N are widely used in soil science, the
473 NanoSIMS is capable of measuring isotope ratios with a precision of $\sim 1\%$ only in very
474 favorable cases, and even a level of $\sim 10\%$ precision is likely to be very challenging to
475 achieve in most complex soil samples. To obtain such a high precision ($< 1\%$), relatively large
476 amounts of material must be extracted from the sample surface (nanograms), requiring a
477 large primary spot size $\sim 20 - 30 \mu\text{m}$. Such a spot size might itself exceed the micro-scale
478 structures of interest (e.g. bacterial cells, clay minerals). Also, the much smaller primary
479 beam used in NanoSIMS imaging generates a smaller number of secondary ions,

480 necessitating the use of electron multiplier (EM) detectors. EMs have a faster response time
481 than faraday cup detectors (FC) (commonly used in larger beam SIMS instruments), and are
482 thus both fast enough and provide sufficient dynamic range for imaging. EM detectors are,
483 however, subject to a number of artefacts (limited count rates and detector aging) that
484 effectively limit the precision to about 1%. On top of this, the extraction conditions from
485 location to location can be hard to maintain at a level that yields precision better than one
486 part in a thousand, especially with heterogeneous samples such as soils. The limitations on
487 precision mean that in most soil systems, natural abundance measurements will not produce
488 useful data. Isotopic measurements with higher precision can be achieved using the Cameca
489 IMS1280, a large-geometry magnetic sector ion probe, combining high transmission, high
490 abundance sensitivity and high density of the primary beam with thermally insulated FC
491 electronics. This instrument could potentially be used in complementary studies with a
492 NanoSIMS to record images of high spatial resolution as well as per mil level precision.

493 In our experience, tracking of isotopically labeled tracers is probably the most practical way
494 to explore micro-scale soil processes using NanoSIMS (Herrmann et al., 2007a; Keiluweit et
495 al., 2012). As C and N are the key elements in organic matter studies, substrates enriched in
496 ^{13}C and/or ^{15}N are regularly used for general investigations of microbial metabolism in soils
497 as well as for the more specific purpose of following the fate of organic compounds as they
498 cycle through soils (Kuzyakov et al., 2000; Ruetting et al., 2011). Of critical importance in
499 tracer studies is whether the labeled substrate becomes chemically modified or is otherwise
500 affected by the sample preparation. The potential user is reminded that NanoSIMS is not well
501 suited for the identification of molecules or characteristic molecular fragments and so will
502 rarely be able to address this kind of problem directly.

503 While quantitative NanoSIMS isotopic analyses are relatively straightforward, quantitative
504 analyses of elemental abundances are considerably more challenging. In the fields of
505 material science and mineralogy, SIMS users usually employ standards to correct for
506 differences in yields and quantity for defined element-matrix combinations. The inherent

507 complexity and variability of soil matrices can complicate this approach, as appropriate
508 standards are harder to obtain or manufacture. The C to N elemental ratio in soil OM, for
509 example, is of general interest to soil scientists. The measurement of this ratio is inherently
510 challenging because $^{12}\text{C}^-$ has a different formation mechanism than the $^{12}\text{C}^{14}\text{N}^-$ ion (N is
511 detected as CN), as atomic N ionization is very poor. As a result, the yield of the two species
512 can change relative to each other during the course of an analysis. C to N ratio
513 measurements are therefore very challenging, requiring matrix-matched standards and
514 method optimization, and ultimately may result in measurements of low accuracy and
515 precision. It is an open question whether the heterogeneity of soil material makes such
516 measurements additionally challenging.

517 3.2. Sample documentation

518 To facilitate the analyses, it is best to determine regions of interest on the sample prior to
519 performing NanoSIMS measurements (Herrmann et al., 2007a; Moore et al., 2011a; Weber
520 and Holt, 2008). Sample mapping can greatly enhance the efficiency of the analyses and is
521 often critical to interpretation of results. Most SIMS instruments have the equivalent of an epi-
522 illumination microscope for sample navigation, and therefore epi-illumination micrographs
523 provide the best reference images for general navigation. Electron microscopy can also
524 positively identify targets for analysis, and these images are often easily comparable to the
525 secondary electron or ion images generated during NanoSIMS analyses. Ideal mapping
526 images range from the whole sample scale to the individual target scale, with reference
527 points that can be used to translate from one image scale to the next.

528

529

530 3.3. Instrument tuning and quality control

531 Here we present a brief introduction to issues that may be encountered during the tuning of a
532 NanoSIMS 50 or 50L; more detailed instructions have been previously published (Pett-Ridge

533 and Weber, 2012). The central aspects of SIMS instrument tuning are mass selection,
534 resolving isobaric interferences and peak shape.

535 a) **Mass selection:** To obtain accurate measurements, the secondary ion mass
536 spectrometer must be tuned and aligned to collect ion masses of interest. Choosing
537 masses will depend entirely upon the question being asked, what isotopically labeled
538 compounds have been added, and whether operation is proceeding in Cs^+ or O^-
539 mode. Often this necessitates choosing between analyzing common bio-elements
540 (e.g. C, N, O, S, P) with a Cs^+ beam, or metals/metalloids (e.g. Fe, Al, Mn, Mo) with a
541 O^- beam. If the ion yield is sufficient, some creative solutions exist, for example Fe
542 can be detected as FeO^- in Cs^+ mode. Alternatively, subsequent O^- mode
543 measurement of the same spot is possible.

544 b) **Isobaric interferences:** When selecting ion masses it is critical to consider and
545 exclude isobaric interferences, which are species with near-identical masses to the
546 species of interest. Isobaric interferences can be problematic for SIMS because the
547 sputtering process generates molecules. Therefore, in addition to isotopes with the
548 same mass (e.g., ^{48}Ti and ^{48}Ca), users must consider isobaric interferences that are
549 clusters of atoms, many of which are artificial (e.g., $^{23}\text{Na}^{24}\text{Mg}^1\text{H}^+$). To identify
550 potentially significant isobaric interferences, the first step is to determine the major
551 elemental composition of the sample (here, previous SIMS studies may be helpful).
552 Blanks and control samples can be used to determine if interfering molecules are
553 produced at significant levels. If this turns out to be the case, the exact masses of
554 significant isobaric interferences need to be calculated relative to the exact mass of
555 the target species to determine difference in mass (ΔM) and the mass resolving
556 power ($\text{MRP} = M/\Delta M$) required to resolve the target species. MRP is a metric of peak
557 shape and the tuning of the mass spectrometer.

558 c) **Peak shape:** The scan of the mass peak should be both flat-topped and steep-sided.
559 The shape of the peak is the cumulative result of everything from the primary beam
560 location and size to the gain on the detector. A tightly focused and well centered

561 primary beam reduces angular aberration and minimizes potential distortions. The
562 secondary ion beam should be aligned relative to all the lenses, slits and apertures in
563 the secondary mass spectrometer in order to maximize transmission and minimize
564 distortion. The entrance slit effectively sets the nominal MRP of the mass
565 spectrometer, and the aperture slit and energy slit are used to steepen the peak side
566 slopes and reach the target MRP by reducing angular and chromatic aberrations.
567 Peak top flatness is important to measurement stability and indicates that 100% of
568 the target species is collected to the exclusion of isobaric interferences. In addition to
569 tuning and alignment issues, peak top flatness is also affected by the electron
570 multiplier gain, high voltage, threshold and deflector settings.

571 Standards are used during the process of setting up the mass spectrometer; they are used
572 for mass selection, quantification, and session to session comparison of transmission, MRP,
573 and elemental or isotopic ratios. Reference materials can be simple (e.g., iron), multi-element
574 standards like the NIST glass standard NBS610 (500 µg/g of most elements), or
575 generated/characterized 'in-house' by characterizing samples through bulk methods and
576 verifying high resolution homogeneity by replicate SIMS analyses. One example is the
577 *Bacillus subtilis* spore sample used by the LLNL NanoSIMS group as a reference standard
578 for C and N isotopic measurements ($^{13}\text{C}/^{12}\text{C} = 0.0110$; $^{15}\text{N}/^{14}\text{N} = 0.00370$). For this standard,
579 isotopic enrichments were determined by bulk analysis at the University of Utah (Finzi-Hart et
580 al., 2009); measurement precision, σ (internal), is ~4 % (2σ) for individual $^{13}\text{C}/^{12}\text{C}$ and
581 $^{15}\text{N}/^{14}\text{N}$. For many soil science applications, the co-occurrence of both mineral and organic
582 phases requires that both a multi-element (NBS 610) and organic phase standard be used.
583 However, when studying complex organo-mineral interfaces, the aim should always be to
584 simultaneously record mineral and organic derived ions to obtain a complete view on the
585 studied mineral surfaces. Caution must also be exercised when applying SIMS to identify
586 specific mineral phases. The count rate of an ion is not directly proportional to the
587 concentration in the mineral. For example, the content of iron influences the secondary ion
588 yield of other elements that are present in the sample. A linear interpolation based on the

589 elemental concentration of the mineral is, therefore, not reasonable (Lehmann, 2003). It is
590 thus advantageous to confirm mineral identity using X-ray techniques or other methods. In
591 cases where quantification of an element is desired, mineral specific standards are
592 necessary.

593 Minerals in soil pose a particular challenge because mineral grains may accumulate an
594 electrical charge under sustained Cs^+ primary ion beam sputtering. The phenomenon can
595 readily be observed in the NanoSIMS because charged regions generate very low secondary
596 electron yields. The area of charge accumulation may still yield secondary ions, but their
597 trajectories through the secondary mass spectrometer will deviate from those of other ions
598 when they have significantly different energy (>10 V difference). As a result, some species
599 may not be detected with the same relative efficiency, resulting in inaccurate measurements.

600 This is primarily an issue for the analysis of negative secondary ions because large numbers
601 of electrons are extracted when the sample surface is bombarded by a beam of Cs^+ ions. At
602 the initiation of analysis, while the metal coating is still intact, charging may not be obvious. In
603 some cases, minerals (e.g., magnetite) or organic material in the sample may provide
604 sufficient charge conductivity to allow analysis. Most organic matter, while insulating in its
605 natural state, becomes conducting under ion bombardment. However, soil particles, even
606 those initially coated with Au, often begin to show evidence of sample charging after ~ 20
607 minutes of analysis, with significantly diminished total ion counts (Pett-Ridge et al., 2012).
608 This effect has been observed in a NanoSIMS study of microaggregates deposited on
609 silicon-nitride windows, where regions free of organic material appeared to undergo the most
610 obvious charging (Remusat et al., 2012).

611 The best way to overcome sample charging is to use a device called an electron flood gun,
612 commonly referred to as the e-gun. Tuning of the e-gun requires significant experience in
613 aligning the electrons with the primary beam on the sample, and in adjusting the voltage to
614 the charge status of the sample. Another challenge is that secondary electron imaging is not
615 possible while the e-gun is in use. Often it is easiest to initially locate particles of interest with
616 secondary electron imaging, and then turn on the e-gun for ion image data collection. When

617 the e-gun is tuned correctly, nonconductive minerals will not charge and the mass peaks will
618 maintain the same level of mass resolution as achieved on a conducting sample. We note
619 that the sample must be covered with a conductive coating for the e-gun to work; electrons
620 that reach the sample outside the analysis area must have a path to ground. The e-gun is not
621 likely to work with samples with significant topography and is not a solution in cases where
622 topography is the proximal cause of charging and ion shadowing. In tests of different mineral
623 types performed at LLNL, using the e-gun increased the ion yield for C and N by as much as
624 a factor of 10. Additional tests showed that isotope ratios of standard reference materials
625 analyzed both with and without the e-gun were not significantly different (Pett-Ridge et al.,
626 2012). Caution is always advisable when interpreting results where charging is possible.

627 3.4. Sample preparation – from single particles to intact soil

628 In the next paragraphs we discuss possible ways to prepare soil samples ranging from
629 primary particles and aggregates to complex intact samples containing microbial and plant
630 tissues.

631 3.4.1. Direct deposition of individual particles and microaggregates

632 Individual soil particles (e.g. clay minerals, particulate OM) as well as microaggregates can
633 be deposited directly onto an analysis support (e.g. Si-wafer, polished metal stubs) and
634 imaged via NanoSIMS provided they have limited topography and remain adhered to the
635 sample support under high vacuum.

636 Such materials may be derived from physical soil fractionation (Eusterhues et al., 2005) or
637 taken directly from a soil suspension (Keiluweit et al., 2012). The application of ultrasound
638 during soil fractionation may destroy natural soil structure and also re-distribute both organic
639 compounds as well as individual mineral particles between physical fractions (Amelung and
640 Zech, 1999; Mueller et al., 2012a). While pretreatments needed to isolate small particles may
641 introduce experimental bias, it may still be desirable to attempt direct observations of small
642 particles or microaggregates, especially when the nature of the research question prohibits
643 the use of C and N-containing fixatives. Samples can be deposited on flat surfaces like

644 polished metal stubs, Si-wafers, gold foil or directly on SEM or TEM grids (Keiluweit et al.,
645 2012; Mueller et al., 2012b). Alternatively, particles can be collected from soil suspensions
646 on gold coated filter discs, a widely used preparation technique in microbiology (Musat et al.,
647 2012). For obvious reasons, the sample support must be chosen with the elements of
648 interest in mind (Si-wafers are not advisable when Si is a target element). In the direct
649 deposition preparation technique, a single layer of small particles/microaggregates should be
650 deposited on the sample support to minimize topography. If the goal is to simultaneously
651 explore both mineral and microbial constituents, fixation of the biological tissues will be
652 necessary (see below for detailed description).

653 3.4.2. Fixation and preparation of organic materials

654 A variety of biological sample types may be of interest to soil scientists, ranging from root or
655 hyphal tissues to bacterial and archaeal cells, protists and microfauna, or decaying plant
656 litter. For all these sample types, preservation of cell structure is important for target
657 identification and to contain mobile organic and inorganic constituents. Sample preparation
658 typically involves stabilization of biological components (fixation), removal of water
659 (dehydration) and salts (derived from growth media or sea/soil water), deposition of the
660 sample on a conductive support (Si wafer, TEM grid) and subsequent whole cell analysis or
661 thin sectioning after embedding. Fixation of biological tissues is a process used to preserve
662 cell morphology from decay and immobilize analytes of interest by increasing molecular
663 mechanical strength or stability. Chemical fixation for imaging analysis is typically performed
664 with aldehydes (e.g., glutaraldehyde, paraformaldehyde, formaldehyde) that cross-link
665 proteins to hold cell structure together during dehydration, (Kuo, 2007; Nunan et al., 2001;
666 Tippkötter and Ritz, 1996). Low temperature methods like flash freezing and high pressure
667 freezing (Chandra and Morrison, 1992; Dykstra and Reuss, 2003; Echlin, 1992) are an
668 alternative in some circumstances if it is critical to preserve the distribution of small
669 molecules and diffusible ions. For biological samples that are to be analyzed intact, collection
670 on a filter is very efficient, and nucleopore or polycarbonate filters can be used as a sample

671 support for SIMS analysis if they are kept flat at the micron scale. Samples grown on a solid
672 sample support can be immersed in fixative and gently washed by repeated immersion in
673 deionized water.

674 If subcellular elemental or isotopic distributions are of interest in soil microbial or plant tissue
675 samples, fixation is often followed by embedding (impregnating the sample with a hard,
676 vacuum stable matrix) and sectioning (cutting the sample into cross-sections) prior to
677 NanoSIMS analysis. Samples can be embedded in a number of polymers for room
678 temperature sectioning (e.g., epoxy, acrylic, paraffin (Dykstra and Reuss, 2003)). Cryogenic
679 sectioning can be performed with sucrose, OCT or similar compounds. Cryosectioning of
680 frozen (water/ice embedded) samples is also an option, but is more technically challenging
681 and requires much practice. Sectioning can be performed with an ultramicrotome, a standard
682 histological microtome or cryostat, or even with a razor blade, depending on the type of pre-
683 NanoSIMS imaging that is desired. An adhesive surface coating (e.g. poly-L-lysine, vector
684 bond, egg white) can be used to retain sections during washing or staining. Such surface
685 coatings can also be used for the fixation of other thin sections or micro-scale single particles
686 on sample mounts (e.g. Me-stubs, Si-wafers). Contrast stains used for TEM imaging of
687 biological ultrastructure (e.g. uranyl acetate) typically are compatible with SIMS because
688 mass spectrometry can easily resolve the stain components from many species of interest.
689 However, there may be cases where contrast stains would be a source of unwanted
690 background counts, particularly for metal analysis. Standard TEM-grade ultrathin sections
691 (~100 nm) can be analyzed by high resolution NanoSIMS, but with a limited analysis time to
692 avoid section breakage or consumption. To extend the SIMS analysis time and collect more
693 data while still allowing correlated TEM-SIMS analysis, thicker sections (up to 500 nm) can
694 be prepared, though with a loss in TEM image quality. Thicker sections are also desirable if
695 large areas (mm^2) need to be analyzed. Focused ion beam (FIB) milling can also be used as
696 an alternative to embedding and sectioning (Weber et al., 2010), particularly where the user
697 needs to have precise control over the location and orientation of the sample thin-section.
698 Thin sections can be laid on a TEM grid or directly on a solid substrate prior to SIMS

699 analysis. For example, this technique was used by Bonneville et al. (2011) to prepare cross
700 sections of a micro-scale fungal hyphae / biotite interface for subsequent TEM analyzes. If
701 transmission light imaging is necessary for sample mapping, indium tin oxide (ITO) coated
702 glass slides are preferable to uncoated glass slides because the ITO coating does not
703 charge under ion bombardment.

704 3.4.3. Preparation of aggregated soil structure and intact plant-soil systems

705 Many soil researchers would like to be able to image cross-sections of both biological and
706 mineral phases in intact plant-soil samples. However, three dimensional multiphase objects
707 often require additional preparation steps that go beyond what is required for a purely
708 organic or purely mineral sample. Essentially, the object of interest needs to be embedded in
709 a solid, vacuum-compatible medium and subsequently cut and or polished to generate a flat
710 surface. The primary distinction between preparation of organic materials (see above) and
711 preparing soil samples, is that cutting heterogeneous samples must accommodate both
712 'hard' (quartz, Fe oxides) and 'soft' components (plant tissues).

713 The most useful approaches for NanoSIMS soil sample preparation fall into three general
714 categories: 1) embedding with resin (epoxy, acrylic, polyester), sucrose or paraffin, 2)
715 embedding in molten elemental sulphur (S), or 3) cryo-techniques. The appropriateness of
716 these three techniques depends on the target elements which are to be analyzed and the
717 size of the sample (microaggregate vs. intact soil core). In general, resin embedding is the
718 most useful approach for larger aggregates and soil cores, whereas cryo-
719 preservation/sectioning and S embedding are the best choices for small (~100 μm)
720 microaggregates. Cryo and S embedding have the added benefit that no artificial C or N is
721 added as background material. We note that it may be possible to subtract a background
722 resin signal from the sample signal using the difference in the CN/C ratio, (e.g. the biological
723 from the non-biological material). The CN/C ratio of resin is quite distinct from that of
724 biological material, so regions representing resin within analysis images can be omitted at
725 the data processing stage (Weber et al., 2012).

726 For larger specimens like macroaggregates (>2 mm) or intact soil cores containing both hard
727 mineral constituents and soft tissues such as plant residues (e.g. roots in Figure 5), microbes
728 and plant roots, resin embedded sections are typically created and then polished for further
729 analyses. One epoxy resin approach was described by (Herrmann et al., 2007a), who
730 developed a technique for the preservation of microbial communities in quartz-based soils
731 that was later modified by Clode et al. (2009) to include plant roots. Infiltration of samples in
732 acetone-epoxy resin mixtures was conducted over a period of days, with the concentration of
733 'Araldite' (epoxy resin) gradually increased until 100%. At a larger spatial scale, at TU
734 München this procedure was successfully applied to prepare natural intact soil cores for
735 NanoSIMS analyses from the permafrost layer of cryoturbated soils (see Figure 2). Previous
736 studies show that the abundance of nitrogenous compounds was not adversely affected by
737 this procedure (Herrmann et al., 2007a; Peteranderl and Lechene, 2004).

738 An alternative to resin embedding is sulfur embedding (De Gregorio et al., 2010; Flynn et al.,
739 2004; Lehmann et al., 2005) which has been successfully used to section heterogeneous soil
740 aggregates (Herrmann et al., 2007a; Lehmann et al., 2005). The most significant benefit of S
741 embedding is that aggregates can be embedded in a non-C based, room temperature
742 sectionable medium. In the DeGregorio et al. (2010) approach, elemental sulphur is heated
743 to its molten state (> 100°C), then a soil aggregate is inserted and allowed to cool. The
744 resulting material can be glued to a metal stub and sectioned using an ultramicrotome.
745 Unfortunately, the sulphur may provide only limited structural integrity for the sections
746 because it tends not to impregnate samples extensively. Also, the high temperature could
747 potentially alter organic materials, particularly those on the surface of the aggregate. A low-
748 temperature alternative, the S embedding approach described by Lehman et al. (2005),
749 consists of S heated until molten and rapidly cooled in liquid N₂. As the S is slowly warmed to
750 room temperature, it goes through a phase of high viscosity and at this stage (~20 seconds)
751 aggregates may be inserted into the S. The resulting S block remains amorphous or plastic
752 for a limited amount of time, during which sectioning should be carried out.

753 A final option for fixation and sectioning is the cryopreservation/sectioning approach used by
754 researchers at LLNL: high-pressure freezing (Leica EMPACT2) of soil aggregates
755 surrounded by ultrapure H₂O in small copper tubes (16.6mm) with an internal diameter of
756 350µm, followed by cryosectioning and freeze drying. This approach results in samples of
757 regular thickness (<400 nm) and minimal chemical changes (Figure 6). This method, though
758 challenging, preserves the distribution of diffusible ions and molecules. Because it involves
759 fast freezing but no cyro-protectant, no background material is introduced that might dilute
760 the C or N isotopic signal (Figure 6).

761 Once a soil sample is embedded, it must then be cut to expose a cross-section for
762 NanoSIMS analysis. The presence of mineral grains significantly increases the difficulty of
763 sectioning samples. While ultramicrotomy with a diamond knife is possible, it is significantly
764 easier to cut embedded soil aggregates and cores with a wafer saw and then polish them as
765 per a geological sample. This is, however, not ideal for some softer biological materials and
766 resins, which can abrade more easily, resulting in topographical differences across the
767 sample surface. This abrasion effect can be particularly pronounced at the edges of mineral
768 grains, where inorganic-organic interfaces are located.

769 Sectioning via ultramicrotomy is the primary alternative option to saw cutting, and has proven
770 highly effective for combined TEM and NanoSIMS stable isotope measurements of plant-soil
771 systems (Clode et al., 2009). In Figure 5, a SEM image of three embedded roots illustrates
772 how the heterogeneous distribution of soft and hard soil compartments can both be
773 preserved in a thin section (Clode et al., 2009). In this procedure, both plant tissues and
774 microorganisms appeared to be well preserved (Figure 4 and Figure 5). We note that the
775 sectioning of embedded soil aggregates with heterogeneous density requires a highly skilled
776 operator; it is easy to chip a diamond knife. A final option for sectioning fixed samples is FIB
777 sectioning. This approach is a particularly good option for preserving the distribution of
778 diffusible species because a fully dry sample can be sectioned, however the method requires

779 specialized equipment and limited sample material can be processed. If the samples are only
780 destined for SIMS analysis, top-cutting is a more rapid FIB option (Weber et al., 2010).

781 3.5. Data acquisition and analysis

782 There are two main data collection modes possible with the NanoSIMS 50; spot
783 measurements and ion images. The collection of secondary ions in the spot mode is usually
784 used for the direct recording of isotopic ratio data for a discrete location. However, the main
785 data collection mode for soil related studies is likely to be ion imaging because users working
786 with highly complex samples are usually interested in spatially explicit isotope ratios and
787 contextual information. NanoSIMS ion image files consist of individual images for each scan
788 (plane) for each given mass, along with metadata describing the conditions of the analysis.
789 There are a number of image processing software options available to analyze the ion image
790 data. WinImage is Cameca's Windows-based image processing package that comes pre-
791 installed with the Windows-based NanoSIMS software. The previous Solaris-based
792 NanoSIMS software featured a somewhat rudimentary ion image processing application
793 called simply, Image. Another software package for SIMS image processing is the Windows
794 based LIMAGE program developed by Larry Nittler at the Carnegie Institution of Washington
795 (independent from Cameca). In addition to these commercial programs there are two open
796 source packages. The NRIMS (National Resource for Imaging Mass Spectrometry) group at
797 Harvard University has developed a plugin for the java-based freeware ImageJ. The so-
798 called MIMS plugin provides a number of specific data processing options in addition to the
799 full range of ImageJ capabilities. Most notable is the ability to express ratio images on a Hue-
800 Saturation-Intensity (HSI) scale, where the scale parameters can be set by the user. Finally,
801 a very recently developed software is the Matlab based application Look@NanoSIMS
802 developed by Lubos Polerecky at the Max-Planck Institute for Marine Microbiology in Bremen
803 (Polerecky et al., 2012). No matter what software is used there are some basic steps for the
804 processing of NanoSIMS images (the sequence of steps may vary slightly for some specific
805 data sets or research questions).

806 Briefly, the first step of image analysis is to examine all obtained images for possible flaws
807 (e.g. spots of charging, unrecorded spots or lines within images). When multiple cycles are
808 recorded, the analyst has to decide whether any cycles should be excluded from further
809 analysis. Individual cycles should be aligned to correct for primary beam drift, and also dead-
810 time corrected. This dead time is the period when the detector has counted a single
811 secondary ion but is not ready to count another (usually tens of nanoseconds). Next, the
812 species of interest are normalized to major element species (e.g. $^{13}\text{C}^-/^{12}\text{C}^-$, or $^{12}\text{C}^-/^{12}\text{C}^{14}\text{N}^-$);
813 ratio images can be used efficiently to evaluate the quality of the ratio data and the
814 distribution of normalized data. Typically, quantitative data are obtained by defining regions
815 of interest (ROIs), which consist of a group of pixels bounding a particular feature. In most
816 image processing applications a ROI can be drawn directly onto the image, and the software
817 then records the sum of the counts from the pixels within the ROI and thus also ratio data.
818 Defining ROIs is a critical step. Without objective criteria, it is possible to change the isotopic
819 enrichments just by changing the size of an ROI. The best ROI selection criteria are external
820 images (e.g. SEM image or fluorescence image) or single ion images (e.g. $^{56}\text{Fe}^{16}\text{O}^-$ for iron
821 oxide particles). Alignment with an external image is possible when using the
822 Look@NanoSIMS software. In many cases, it is necessary to visually evaluate the spatial
823 distribution of several ions to interpret and properly define ROI's. Unfortunately, there are no
824 standard procedures for feature selection in complex matrices like soils.

825 After ROIs are defined, the data can be extracted and interpreted. One promising way to
826 evaluate micro-scale ion images might be use of geostatistics, which are often used for
827 larger plot or ecosystem analyses (Steffens et al., 2008). Geostatistics can be used to
828 identify dependencies within any spatial data (e.g. NanoSIMS ion images). For example it
829 might be possible to use this approach to evaluate the spatial distribution of Fe within a
830 complex soil matrix. Figure 7 illustrates the application of a statistical approach (R 2.13.1 (R
831 Development Core Team, 2011) in combination with the g-stat 2.4.0 package (Pebesma,
832 2004) to evaluate spatial dependencies between organic matter ($^{12}\text{C}^{14}\text{N}^-$) and particles
833 containing iron ($^{56}\text{Fe}^{16}\text{O}$). The analysis is based on data extracted from a 32 μm line scan

834 drawn on the NanoSIMS images (Figure 7 A and B). The sample is a Cambisol soil
835 aggregate embedded in Araldite, originally from Höglwald, Bavaria, Germany. Both
836 semivariograms for $^{12}\text{C}^{14}\text{N}^-$ and $^{56}\text{Fe}^{16}\text{O}^-$ (Figure 7 C and D) show a comparable periodic
837 behavior, where the semivariance is oscillating (y-axis). The semivariance is a measure of
838 spatial dissimilarity. Thus the wave like appearance of the semivariance demonstrates a
839 distinct spatial pattern of similar ion counts ($^{12}\text{C}^{14}\text{N}^-$ and $^{56}\text{Fe}^{16}\text{O}^-$) and thus a regularity in the
840 aggregate architecture (organic and mineral spheres). But as the spatial frequency (x-axis) of
841 the maxima and minima of the semivariance is different between $^{12}\text{C}^{14}\text{N}^-$ and $^{56}\text{Fe}^{16}\text{O}^-$, this
842 indicates differences in spatial structures and different pattern sizes. This analysis indicated
843 that iron clusters ($^{56}\text{Fe}^{16}\text{O}^-$) are spatially independent from organic matter ($^{12}\text{C}^{14}\text{N}^-$). Similar
844 analyses may be particularly useful to reveal spatial inter-dependencies between mineral and
845 organic soil constituents or even between areas enriched or depleted in specific stable
846 isotopes. Another approach to NanoSIMS data analysis is the upscaling approach used by
847 Fike and colleagues (Fike et al., 2008). They collected numerous single spot (6 μm x 6 μm)
848 NanoSIMS measurements (>300) and measured the isotopic variability of sulfide within the
849 oxycline of a cyanobacterial mat (sampling grids: 3500 μm by 450 μm and 3000 μm by 500
850 μm , spatial increment of 50-200 μm). Analyzing the $\delta^{34}\text{S}$ abundance and isotopic
851 fractionation, they observed fine scale laminations (1 to 400 μm) and clear zonation. This
852 work suggests that single spot NanoSIMS measurements, collected on up to a millimeter
853 scale and linearly interpolated, could be applied for upscaling micrometer spot data in soils.

854 4. Combination with other micro-scale techniques

855 4.1. Scanning and transmission electron microscopy

856 Prior to the development of NanoSIMS, electron microscopy was the approach of choice for
857 the observation of soil particle arrangements (Gillott, 1970; Gray, 1967; Howard et al., 1996;
858 Kowalkowski and Mycielskadowgiallo, 1985). Electron microscopy has evolved to achieve
859 very high resolution, touching on 1 nm in scanning electron microscopy (SEM) and 0.05 nm
860 in transmission electron microscopy (TEM). Similar to NanoSIMS, electron microscopy

861 techniques can be used to obtain information about the material properties of a sample, in
862 addition to providing an image. In a scanning electron microscope (SEM), a high energy
863 focused beam of electrons is produced. The electrons interact with electrons in the sample,
864 producing secondary electrons, back scattered electrons (BSE), and characteristic X-rays
865 (Energy-dispersive X-Ray Spectroscopy EDX/EDS/EDXS) that can be detected and that
866 deliver information about the sample's surface topography and composition. An SEM-BSE
867 image is a good tool to differentiate between organic and mineral spheres. This can be useful
868 in samples without topography such as polished soil cross sections. The crystalline state of a
869 sample can be determined by recording patterns of the diffracted backscattered electrons
870 (EBSD) and matching them with a data base for crystallographic structures. An EDX scan
871 yields information on the localization of minerals versus organic matter and is useful for
872 identifying regions of interest within the sample.

873 It should be noted however, that in contrast to NanoSIMS, where information is gathered only
874 from secondary ions sputtered from the uppermost atomic layers, the interaction volume of
875 secondary ions in SEM extends in a pear shaped fashion between 100 nm and 5 µm deep
876 into the sample (depending on the energy of the electron beam, atomic number and density
877 of the specimen). EDX is therefore not a surface technique *sensu strictu* and it has been
878 shown that TEM maps do not always compare well with subsequently obtained NanoSIMS
879 images (Badro et al., 2007).

880 4.2. Synchrotron based techniques

881 To study soil process dynamics as a function of location within aggregates and
882 microaggregates, simultaneous information on (a) localization, (b) identification and (c)
883 transformation of organic matter and mineral phases is required with very high spatial
884 resolution. Conventional electron microscopes can visualize basic elemental composition but
885 are unable to speciate carbon compounds. A number of techniques can yield data on C
886 composition (ion microprobe laser desorption, laser ionization mass spectrometry, Raman
887 microscopy, ¹³C-NMR, FTIR (Lehmann et al., 2005; Lehmann et al., 2009), though few can

888 provide molecular or elemental characterization with the sub-micron resolution necessary to
889 study mineral-organic interactions in microaggregates. These goals can be approximated
890 with the combination of NanoSIMS and Scanning Transmission X-ray Microscopy, Near
891 Edge X-ray Absorption Fine Structure Spectroscopy (STXM/NEXAFS). The resolution of
892 synchrotron based X-ray microscopes can approach 50 nm, comparable to the NanoSIMS
893 spot size. Raster scan images can be obtained at energy spacings of ~0.1 eV across 100's
894 of eV energy ranges. The spatially resolved NEXAFS spectra extracted from the respective
895 image 'stacks' reveal the bonding environment of the element of interest, allowing the
896 speciation of organic matter forms and elemental redox states. STXM/NEXAFS has been
897 used successfully to describe spatial patterns and speciation of soil organic matter
898 associated carbon (Bardgett et al., 2007; Cheng et al., 2008a; Cheng et al., 2008b; Lehmann
899 et al., 2005), and nitrogen (Gillespie et al., 2009; Kögel-Knabner et al., 2008; Sleutel et al.) in
900 a broad range of environments, including marine systems (Brandes et al., 2004).

901 A combined 'STXM-SIMS' approach allows precise, quantitative measurement of molecular
902 and isotopic patterns in undisturbed samples, at high resolution (Keiluweit et al., 2012; Pett-
903 Ridge et al., 2012). By combining NanoSIMS with STXM/NEXAFS it is possible to map
904 organic C distribution, to image associations of organics with specific mineral types, and to
905 trace organic matter of variable origin into the soil matrix (Lehmann et al., 2007; Wan et al.,
906 2007). If combined with isotope tracer experiments, the images acquired through this
907 approach can document the forms of C that become stored in soil aggregates and
908 simultaneously track microbial debris and other organic polymers into the soil matrix.

909 Technical challenges to the combined application of STXM and NanoSIMS have recently
910 been summarized by Pett-Ridge et al. (2012). They point out that experimental activities
911 have to be planned in a way such that STXM analysis precedes NanoSIMS, as the latter
912 method has a much greater potential for destructive interference with the sample. Sample
913 holders commonly used in synchrotron spectroscopy may contain N (Si_3N_4) or C (TEM Cu
914 grids with C lacey) and must therefore be chosen to avoid unwanted secondary ion species

915 (e.g. $^{12}\text{C}^-$, $^{12}\text{C}^{14}\text{N}^-$) in subsequent NanoSIMS applications. Samples cannot be significantly
916 thicker than 150-200 nm for STXM/NEXAFS or they will be impenetrable for soft X-rays. This
917 limits the type of microstructures that can be observed with both methods at the same time to
918 thin platelet-like objects. Taking these restrictions into account, SEM, NanoSIMS and STXM
919 may be applied to the identical soil sample specimen, providing information that is
920 complementary: SEM may be used to generate a mesoscale surface image of the region of
921 interest (ROI), STXM/NEXAFS imaging can obtain information about whole sample
922 chemistry, and NanoSIMS analysis can yield elemental/isotopic data on either surface
923 characteristics or from a depth profile (Pett-Ridge et al., 2012) (Figures 6, 8). To allow for
924 high-resolution SIMS imaging and STXM/NEXAFS spectromicroscopic analysis of the same
925 sample, a specimen must be prepared with limited topography, able to withstand high
926 vacuum, be dry, conductive, thin enough to allow photon transmission ($<1\ \mu\text{m}$), and prepared
927 without carbon-based reagents.

928 An example for the synergistic application of NanoSIMS and STXM/NEXAFS was recently
929 presented by Keiluweit et al. (2012). These authors employed NanoSIMS to follow the fate of
930 isotopically labeled amino sugars from fungal cell walls as they became metabolized or
931 bound to minerals and SOM. Concurrently, STXM/NEXAFS spectromicroscopy was used to
932 determine the chemical transformations of substrate C and N functionalities during the
933 process (Figure 8). The authors determined that ^{15}N -labeled amide N derived from fungal cell
934 wall material preferentially associated with Fe (hydr)oxide surfaces or Fe-OM coprecipitates
935 on the surface of other minerals. Through the combination of NanoSIMS and STXM/NEXAFS
936 it was further possible to determine that amide N found on mineral surfaces originated from
937 bacterial protein rather than from the original amino sugars or from nucleotides. This
938 example illustrates that combined applications of synergistic imaging techniques such as
939 NanoSIMS and STXM have the potential to provide information about organic matter-
940 mineral-microbial relationships while avoiding the artifacts inevitably generated by chemical
941 or physical fractionation procedures.

942 4.3. Atomic force microscopy

943 The atomic force microscope (AFM) is another tool for imaging, measuring, and manipulating
944 matter at the nanoscale. An AFM consists of a cantilever with a sharp tip that is used to scan
945 the specimen surface. When the tip is brought into proximity of a sample surface, forces
946 between the tip and the sample lead to a deflection of the cantilever. The deflection of the
947 cantilever is measured and converted to an image of the sample surface. Reports on AFM
948 applications in soil science are increasing (Cheng et al., 2008c; Rennert et al., 2012;
949 Schaumann and Mouvenchery, 2012; Totsche et al., 2010) and typically provide information
950 about local topography and properties of minerals and soil aggregates surfaces at very high
951 spatial resolution. To date, the focus of soil related AFM work has been on interactions
952 between microorganisms and minerals, mainly iron oxides and hydroxides (Maurice, 1996;
953 Maurice et al., 2000). Balogh-Brunstad et al. (2008) combined SEM and AFM to investigate
954 fungal weathering of biotite in a batch liquid culture.

955 One potential combined AFM-NanoSIMS application could be the use of AFM to correct for
956 topography effects in NanoSIMS analyses. Here AFM would be applied both before and after
957 SIMS, allowing the user to convert SIMS data into a true three-dimensional representation of
958 the analyzed species (Fleming et al., 2011). Wirtz et al. (2012a; 2012b) report the
959 development of an integrated SIMS- scanning probe microscope (SPM). In this instrument, a
960 specially developed SPM system was integrated in a Cameca NanoSIMS 50, allowing the
961 user to record topographical *in situ* images of the sample surface before, in between and
962 after SIMS analysis.

963 4.4. In situ single-cell labeling

964 Environmental microbiologists see particular value in the combination of *in situ* phylogenetic
965 labeling and NanoSIMS in order to link metabolic function with taxonomic identity (Kuypers
966 and Jorgensen, 2007). This capacity was first demonstrated using a combination of
967 conventional SIMS and fluorescence *in situ* hybridisation (FISH) to analyze an archaeal-

968 bacterial consortium in anoxic marine sediments (Orphan et al., 2001). The FISH-SIMS
969 combination allowed Orphan et al. (2001) to demonstrate that cell aggregates binding a
970 specific archeal probe were strongly depleted in ^{13}C , indicating a methane-based
971 metabolism. In many natural microbial systems, this approach may be even better suited to
972 NanoSIMS, as it can provide this information at the length-scale of an individual bacterium
973 ($\sim 1\ \mu\text{m}$). Two variations of this approach are currently used: element-labeled fluorescent *in*
974 *situ* hybridization (EL-FISH) where catalyzed reporter deposition FISH (CARD-FISH) is used
975 to deposit high concentrations of fluorine-containing fluorophores in target cells (Behrens et
976 al., 2008); or halogen-labeled *in situ* hybridisation (HISH) where a standard FISH protocol is
977 used in combination with halogen (I, Br) tagged probes (Li et al., 2008). NanoSIMS can then
978 be used to visualize the labeled cells by acquiring a signal for ^{19}F , which is not naturally
979 present at high concentrations in most environmental cells (Behrens et al., 2008; Halm et al.,
980 2009; Musat et al., 2008). In these approaches, a phylogenetic probe is linked to a highly
981 electronegative elemental label (fluorine, iodine, gold, selenium, or bromine) instead of the
982 typical fluorophore, which can be detected in concert with ^{13}C and ^{15}N isotopes for functional
983 characterization. These approaches enable simultaneous localization of the tag and chemical
984 mapping in the NanoSIMS. It may even be possible to use FISH-SIMS approaches in
985 embedded samples (Woebken et al., 2012). The work of Lemaire et al. (2008), where fixed
986 samples were embedded in TissueTek® (Sakura Finetek Labware & Accessories) and then
987 cryosectioned and FISH labeled, suggests this may be possible. However, its usefulness in
988 soil may be limited unless a means to overcome soil's natural background fluorescence is
989 developed. Also, care must be taken with quantitative interpretation of FISH-SIMS results,
990 since these approaches may reduce the original cell enrichment by 60-80% for ^{13}C and 30-
991 60% for ^{15}N (J. Pett-Ridge and S. Behrens, unpublished data).

992 **5. Conclusion**

993 Over the last decades soil scientists have gained a working knowledge of fundamental soil
994 processes ranging from the stabilization of organic matter to microbial diversity in soils. We

995 are now able to track the fate of specific molecular plant biomarkers into organo-mineral
996 associations and to determine the microbial communities responsible for the turnover of
997 specific organic compounds. However, commonly used bulk analyses average over a vast
998 swath of microbial and mineral landscapes, and can miss micro-scale phenomena caused by
999 specific micro-habitats or distinct spatial heterogeneities in the formation of organo-mineral
1000 assemblages. Thus, while our knowledge of bulk scale biogeochemical soil processes is
1001 expanding, we have lacked the high resolution techniques needed to illustrate the
1002 mechanistic underpinnings such processes in intact soil structures.

1003 The emerging class of nano- and microscale spectroscopy and spectrometry techniques has
1004 opened a new frontier in the effort to develop a fundamental understanding of soil processes.
1005 Though the first review of NanoSIMS in soil ecology and biogeochemistry by Herrmann and
1006 colleagues was in 2007 (Herrmann et al., 2007b), this field is still in its early phases as soil
1007 scientists grapple with the many technical challenges. Looking forward, the challenge will be
1008 upscaling from micro-scale analyses to scales from the soil horizon or even to the pedon or
1009 ecosystem scale. These leaps may not come soon, but for now the ability to image elements
1010 and stable isotopes at a previously unresolved spatial scale permits the combination of
1011 established isotopic enrichment techniques with the description of their spatial distribution in
1012 soil microenvironments. Recently, several new NanoSIMS instruments have been installed
1013 and the access for soil scientists is increasing. NanoSIMS analyses have the potential to
1014 contribute to a fundamentally new understanding of soil processes, one that is rooted at the
1015 relevant scale of microbial, mineral and organic matter interactions.

1016 **Acknowledgements**

1017 The authors thank H. Lugmeier, M. Hanzlik, M. Keiluweit, J. Bougoure, and P. Nico for their
1018 help and support with imaging. The oak clones were cultivated by the group of F. Buscot at
1019 the UFZ in Halle, Germany. The oak root experiment was carried out together with T. Grams
1020 and O. Angay and the samples were prepared by M. Greiner. The sampling campaign of the
1021 Alaskan samples was funded by the NSF Postdoctoral Fellowship in Polar Regions

1022 Research (#0852036) and the DFG “Initiation of International Cooperations” (MU 3021/2-1).
1023 We thank J. Kao-Kniffin, J. Bockheim and K. Hinkel for their help with sampling and sample
1024 preparation of the Alaskan samples. We thank M. Steffens for his assistance in geostatistics.
1025 The NanoSIMS instrument at TUM was funded by DFG (KO 1035/38-1). Work of P.K. Weber
1026 and J. Pett-Ridge was performed under the auspices of the U.S. Department of Energy by
1027 Lawrence Livermore National Laboratory under Contract DE-AC52-07NA27344, with funding
1028 provided by an LDRD “Microbes and Minerals: Imaging C Stabilization” at LLNL to JPR and
1029 PKW.
1030

1031 References

- 1032** Amelung, W., and Zech, W. (1999). Minimisation of organic matter disruption during particle-size
1033 fractionation of grassland epipedons. *Geoderma* **92**, 73-85.
- 1034** Audinot, J. N., Schneider, S., Yegles, M., Hallegot, P., Wennig, R., and Migeon, H. N. (2004). Imaging of
1035 arsenic traces in human hair by nano-SIMS 50. *Applied Surface Science* **231**, 490-496.
- 1036** Badro, J., Ryerson, F. J., Weber, P. K., Ricolleau, A., Fallon, S. J., and Hutcheon, I. D. (2007). Chemical
1037 imaging with NanoSIMS: A window into deep-Earth geochemistry. *Earth and Planetary*
1038 *Science Letters* **262**, 543-551.
- 1039** Balesdent, J., Chenu, C., and Balabane, M. (2000). Relationship of soil organic matter dynamics to
1040 physical protection and tillage. *Soil & Tillage Research* **53**, 215-230.
- 1041** Bardgett, R. D., Richter, A., Bol, R., Garnett, M. H., Baumler, R., Xu, X. L., Lopez-Capel, E., Manning, D.
1042 A. C., Hobbs, P. J., Hartley, I. R., and Wanek, W. (2007). Heterotrophic microbial communities
1043 use ancient carbon following glacial retreat. *Biology Letters* **3**, 487-490.
- 1044** Behrens, S., Losekann, T., Pett-Ridge, J., Weber, P. K., Ng, W.-O., Stevenson, B. S., Hutcheon, I. D.,
1045 Relman, D. A., and Spormann, A. M. (2008). Linking Microbial Phylogeny to Metabolic Activity
1046 at the Single-Cell Level by Using Enhanced Element Labeling-Catalyzed Reporter Deposition
1047 Fluorescence In Situ Hybridization (EL-FISH) and NanoSIMS. *Appl. Environ. Microbiol.* **74**,
1048 3143-3150.
- 1049** Billings, S. A., and Richter, D. D. (2006). Changes in stable isotopic signatures of soil nitrogen and
1050 carbon during 40 years of forest development. *Oecologia* **148**, 325-333.
- 1051** Blair, N., Prince, K. E., Faulkner, R. D., and Till, A. R. (2006). Using the scanning electron microprobe
1052 and secondary ion mass spectrometry to locate C-14- and C-13-labelled plant residues within
1053 soil aggregates. *Scanning* **28**, 259-266.
- 1054** Bonneville, S., Morgan, D. J., Schmalenberger, A., Bray, A., Brown, A., Banwart, S. A., and Benning, L.
1055 G. (2011). Tree-mycorrhiza symbiosis accelerate mineral weathering: Evidences from
1056 nanometer-scale elemental fluxes at the hypha-mineral interface. *Geochimica Et*
1057 *Cosmochimica Acta* **75**, 6988-7005.
- 1058** Bradl, H. B. (2004). Adsorption of heavy metal ions on soils and soils constituents. *Journal of Colloid*
1059 *and Interface Science* **277**, 1-18.
- 1060** Brandes, J. A., Lee, C., Wakeham, S., Peterson, M., Jacobsen, C., Wirick, S., and Cody, G. (2004).
1061 Examining marine particulate organic matter at sub-micron scales using scanning
1062 transmission X-ray microscopy and carbon X-ray absorption near edge structure
1063 spectroscopy. *Marine Chemistry* **92**, 107-121.
- 1064** Breland, T. A., and Bakken, L. R. (1991). Microbial growth and nitrogen immobilization in the root
1065 zone of barley (*Hordeum vulgare* L.), Italian ryegrass (*Lolium multiflorum* Lam.), and white
1066 clover (*Trifolium repens* L.). *Biology and Fertility of Soils* **12**, 154-160.
- 1067** Bullock, P., and Murphy, C. P. (1980). Towards the quantification of soil structure. *Journal of*
1068 *Microscopy-Oxford* **120**, 317-328.

- 1069** Bundt, M., Widmer, F., Pesaro, M., Zeyer, J., and Blaser, P. (2001). Preferential flow paths: biological
1070 'hot spots' in soils. *Soil Biology & Biochemistry* **33**, 729-738.
- 1071** Carbol, P., Solatie, D., Erdmann, N., Nysten, T., and Betti, M. (2003). Deposition and distribution of
1072 Chernobyl fallout fission products and actinides in a Russian soil profile. *Journal of*
1073 *Environmental Radioactivity* **68**, 27-46.
- 1074** Chabbi, A., Kogel-Knabner, I., and Rumpel, C. (2009). Stabilised carbon in subsoil horizons is located
1075 in spatially distinct parts of the soil profile. *Soil Biology & Biochemistry* **41**, 256-261.
- 1076** Chandra, S., and Morrison, G. H. (1992). Sample preparation of animal tissues and cell cultures for
1077 secondary ion mass spectrometry (SIMS) microscopy. *Biology of the Cell* **74**, 31-42.
- 1078** Cheng, C. H., Lehmann, J., and Engelhard, M. H. (2008a). Natural oxidation of black carbon in soils:
1079 Changes in molecular form and surface charge along a climosequence. *Geochimica et*
1080 *Cosmochimica Acta* **72**, 1598-1610.
- 1081** Cheng, C. H., Lehmann, J., Thies, J. E., and Burton, S. D. (2008b). Stability of black carbon in soils
1082 across a climatic gradient. *Journal of Geophysical Research-Biogeosciences* **113**.
- 1083** Cheng, S., Bryant, R., Doerr, S. H., Williams, P. R., and Wright, C. J. (2008c). Application of atomic
1084 force microscopy to the study of natural and model soil particles. *Journal of Microscopy-*
1085 *Oxford* **231**, 384-394.
- 1086** Christensen, B. T. (2001). Physical fractionation of soil and structural and functional complexity in
1087 organic matter turnover. *European Journal of Soil Science* **52**, 345-353.
- 1088** Cliff, J. B., Bottomley, P. J., Gaspar, D. J., and Myrold, D. D. (2007). Nitrogen mineralization and
1089 assimilation at millimeter scales. *Soil Biology & Biochemistry* **39**, 823-826.
- 1090** Cliff, J. B., Bottomley, P. J., Haggerty, R., and Myrold, D. D. (2002a). Modeling the effects of diffusion
1091 limitations on nitrogen-15 isotope dilution experiments with soil aggregates. *Soil Science*
1092 *Society of America Journal* **66**, 1868-1877.
- 1093** Cliff, J. B., Gaspar, D. J., Bottomley, P. J., and Myrold, D. D. (2002b). Exploration of inorganic C and N
1094 assimilation by soil microbes with time-of-flight secondary ion mass spectrometry. *Applied*
1095 *and Environmental Microbiology* **68**, 4067-4073.
- 1096** Clode, P. L., Kilburn, M. R., Jones, D. L., Stockdale, E. A., Cliff, J. B., Herrmann, A. M., and Murphy, D.
1097 V. (2009). In situ mapping of nutrient uptake in the rhizosphere using nanoscale secondary
1098 ion mass spectrometry. *Plant Physiology* **151**, 1751-1757.
- 1099** De Gregorio, B. T., Stroud, R. M., Nittler, L. R., Alexander, C. M. O. D., Kilcoyne, A. L. D., and Zega, T. J.
1100 (2010). Isotopic anomalies in organic nanoglobules from Comet 81P/Wild 2: Comparison to
1101 Murchison nanoglobules and isotopic anomalies induced in terrestrial organics by electron
1102 irradiation. *Geochimica Et Cosmochimica Acta* **74**, 4454-4470.
- 1103** Dechesne, A., Pallud, C., and Grundmann, G. L. (2007). "Spatial distribution of bacteria at the
1104 microscale in soil."
- 1105** Dekas, A. E., Poretsky, R. S., and Orphan, V. J. (2009). Deep-Sea Archaea Fix and Share Nitrogen in
1106 Methane-Consuming Microbial Consortia. *Science* **326**, 422-426.

- 1107** DeRito, C. M., Pumphrey, G. M., and Madsen, E. L. (2005). Use of field-based stable isotope probing
1108 to identify adapted populations and track carbon flow through a phenol-degrading soil
1109 microbial community. *Appl Environ Microbiol* **71**, 7858-7865.
- 1110** Derrien, D., Marol, C., Balabane, M., and Balesdent, J. (2006). The turnover of carbohydrates in a
1111 cultivated soil estimated by ¹³C natural abundances. *European Journal of Soil Science* **57**,
1112 547-557.
- 1113** Dykstra, M. J., and Reuss, L. E., eds. (2003). "Biological Electron Microscopy: Theory, Techniques and
1114 Troubleshooting." Kluwer Academic/Plenum Publishers, New York.
- 1115** Echlin, P. (1992). "Low-Temperature Microscopy and Analysis," Springer, New York.
- 1116** Ehleringer, J. R., Buchmann, N., and Flanagan, L. B. (2000). Carbon isotope ratios in belowground
1117 carbon cycle processes. *Ecological Applications* **10**, 412-422.
- 1118** Eickhorst, T., and Tippkoetter, R. (2008). Detection of microorganisms in undisturbed soil by
1119 combining fluorescence in situ hybridization (FISH) and micropedological methods. *Soil*
1120 *Biology & Biochemistry* **40**, 1284-1293.
- 1121** Eusterhues, K., Rumpel, C., and Kögel-Knabner, I. (2005). Organo-mineral associations in sandy acid
1122 forest soils: importance of specific surface area, iron oxides and micropores. *European*
1123 *Journal of Soil Science* **56**, 753-763.
- 1124** Eybe, T., Audinot, J. N., Bohn, T., Guignard, C., Migeon, H. N., and Hoffmann, L. (2008). NanoSIMS 50
1125 elucidation of the natural element composition in structures of cyanobacteria and their
1126 exposure to halogen compounds. *Journal of Applied Microbiology* **105**, 1502-1510.
- 1127** Eybe, T., Bohn, T., Audinot, J. N., Udelhoven, T., Cauchie, H. M., Migeon, H. N., and Hoffmann, L.
1128 (2009). Uptake visualization of deltamethrin by NanoSIMS and acute toxicity to the water
1129 flea *Daphnia magna*. *Chemosphere* **76**, 134-140.
- 1130** Fike, D. A., Gammon, C. L., Ziebis, W., and Orphan, V. J. (2008). Micron-scale mapping of sulfur cycling
1131 across the oxycline of a cyanobacterial mat: a paired nanoSIMS and CARD-FISH approach.
1132 *Isme Journal* **2**, 749-759.
- 1133** Finlay, R., Wallander, H., Smits, M., Holmstrom, S., Van Hees, P., Lian, B., and Rosling, A. (2009). The
1134 role of fungi in biogenic weathering in boreal forest soils. *Fungal Biology Reviews* **23**, 101-
1135 106.
- 1136** Finzi-Hart, J., Pett-Ridge, J., Weber, P., Popa, R., Fallon, S. J., Gunderson, T., Hutcheon, I., Nealon, K.,
1137 and Capone, D. G. (2009). Fixation and fate of carbon and nitrogen in *Trichodesmium* IMS101
1138 using nanometer resolution secondary ion mass spectrometry (NanoSIMS). *Proceedings of*
1139 *the National Academy of Sciences, USA* **106**, 6345-6350.
- 1140** Fisk, A. C., Murphy, S. L., and Tate, R. L. (1999). Microscopic observations of bacterial sorption in soil
1141 cores. *Biology and Fertility of Soils* **28**, 111-116.
- 1142** Fleming, Y., Wirtz, T., Gysin, U., Glatzel, T., Wegmann, U., Meyer, E., Maier, U., and Rychen, J. (2011).
1143 Three dimensional imaging using secondary ion mass spectrometry and atomic force
1144 microscopy. *Applied Surface Science* **258**, 1322-1327.

- 1145** Floss, C., Stadermann, F. J., Bradley, J. P., Dai, Z. R., Bajt, S., Graham, G., and Lea, A. S. (2006).
1146 Identification of isotopically primitive interplanetary dust particles: A NanoSIMS isotopic
1147 imaging study. *Geochimica Et Cosmochimica Acta* **70**, 2371-2399.
- 1148** Flynn, G. J., Keller, L. P., Jacobsen, C., and Wirick, S. (2004). An assessment of the amount and types
1149 of organic matter contributed to the Earth by interplanetary dust. *Advances in Space*
1150 *Research* **33**, 57-66.
- 1151** Gea, L., Jauneau, A., and Vian, B. (1994). Preliminary SIMS imaging of Calcium distribution in
1152 ectomycorrhizas of *Pinus pinaster* and *Hebeloma cylindrosporum*. *Journal of Trace and*
1153 *Microprobe Techniques* **12**, 323-329.
- 1154** Gillespie, A. W., Walley, F. L., Farrell, R. E., Leinweber, P., Schlichting, A., Eckhardt, K. U., Regier, T. Z.,
1155 and Blyth, R. I. R. (2009). Profiling Rhizosphere Chemistry: Evidence from Carbon and
1156 Nitrogen K-Edge XANES and Pyrolysis-FIMS. *Soil Science Society of America Journal* **73**, 2002-
1157 2012.
- 1158** Gillott, J. E. (1970). Fabric of Leda clay investigated by optical, electron-optical, and x-ray diffractions
1159 methods. *Engineering Geology* **4**, 133-&.
- 1160** Grandy, A. S., and Neff, J. C. (2008). Molecular C dynamics downstream: The biochemical
1161 decomposition sequence and its impact on soil organic matter structure and function.
1162 *Science of the Total Environment* **404**, 297-307.
- 1163** Gray, T. R. G. (1967). Stereoscan electron microscopy of soil microorganisms. *Science* **155**, 1668-&.
- 1164** Halm, H., Musat, N., Lam, P., Langlois, R., Musat, F., Peduzzi, S., Lavik, G., Schubert, C. J., Singha, B.,
1165 LaRoche, J., and Kuypers, M. M. M. (2009). Co-occurrence of denitrification and nitrogen
1166 fixation in a meromictic lake, Lake Cadagno (Switzerland). *Environmental Microbiology* **11**,
1167 1945-1958.
- 1168** Hatton, P.-J., Remusat, L., Zeller, B., and Derrien, D. (2012). A multi-scale approach to determine
1169 accurate elemental and isotopic ratios by nano-scale secondary ion mass spectrometry
1170 imaging. *Rapid Communications in Mass Spectrometry* **26**, 1363-1371.
- 1171** Heister, K., Höschen, C., Pronk, G. J., Müller, C. W., and Kögel-Knabner, I. (2012). NanoSIMS as a tool
1172 for characterizing soil model compounds and organomineral associations in artificial soils.
1173 *Journal of Soils and Sediments* **12**, 35-47.
- 1174** Herrmann, A. M., Clode, P. L., Fletcher, I. R., Nunan, N., Stockdale, E. A., O'Donnell, A. G., and Murphy,
1175 D. V. (2007a). A novel method for the study of the biophysical interface in soils using nano-
1176 scale secondary ion mass spectrometry. *Rapid Communications in Mass Spectrometry* **21**, 29-
1177 34.
- 1178** Herrmann, A. M., Ritz, K., Nunan, N., Clode, P. L., Pett-Ridge, J., Kilburn, M. R., Murphy, D. V.,
1179 O'Donnell, A. G., and Stockdale, E. A. (2007b). Nano-scale secondary ion mass spectrometry -
1180 A new analytical tool in biogeochemistry and soil ecology: A review article. *Soil Biology and*
1181 *Biochemistry* **39**, 1835-1850.
- 1182** Hillion, F., Daigne, B., Girard, F., and Slodzian, G. (1993). A new high performance instrument: the
1183 Cameca NanoSIMS 50. In "Secondary Ion Mass Spectrometry" (A. Benninghoven, Y. Nihei, R.
1184 Shimizu and H. W. Werner, eds.), pp. 254-257. Wiley, New York.

- 1185** Hinsinger, P., Bengough, A. G., Vetterlein, D., and Young, I. M. (2009). Rhizosphere: biophysics,
1186 biogeochemistry and ecological relevance. *Plant and Soil* **321**, 117-152.
- 1187** Hoppe, P. (2006). NanoSIMS: A new tool in cosmochemistry. *Applied Surface Science* **252**, 7102-7106.
- 1188** Howard, J. L., Amos, D. F., and Daniels, W. L. (1996). Micromorphology and dissolution of quartz sand
1189 in some exceptionally ancient soils. *Sedimentary Geology* **105**, 51-62.
- 1190** Keiluweit, M., Bougoure, J. J., Zeglin, L. H., Myrold, D. D., Weber, P. K., Pett-Ridge, J., Kleber, M., and
1191 Nico, P. S. (2012). Nano-scale Investigation of the Association of Microbial Nitrogen residues
1192 with Iron (hydr)oxides in a Forest Soil O-horizon. *Geochimica et Cosmochimica Acta* **in press**.
- 1193** Kiczka, M., Wiederhold, J. G., Frommer, J., Voegelin, A., Kraemer, S. M., Bourdon, B., and
1194 Kretzschmar, R. (2011). Iron speciation and isotope fractionation during silicate weathering
1195 and soil formation in an alpine glacier forefield chronosequence. *Geochimica Et*
1196 *Cosmochimica Acta* **75**, 5559-5573.
- 1197** Kips, R. S. E., Weber, P. K., Zavarin, M., Jacobsen, B., Felmy, A. R., and Kersting, A. B. (2012).
1198 Plutonium transport through vadose zone sediments at the Hanford Site: A NanoSIMS study.
1199 In "Plutonium Futures", Cambridge England.
- 1200** Kögel-Knabner, I., Guggenberger, G., Kleber, M., Kandeler, E., Kalbitz, K., Scheu, S., Eusterhues, K.,
1201 and Leinweber, P. (2008). Organo-mineral associations in temperate soils: Integrating
1202 biology, mineralogy, and organic matter chemistry. *Journal of Plant Nutrition and Soil*
1203 *Science-Zeitschrift Fur Pflanzenernahrung Und Bodenkunde* **171**, 61-82.
- 1204** Kowalkowski, A., and Mycielskadowgiallo, E. (1985). Weathering of quartz grains in the liquefied
1205 horizon of permafrost solonchaks in the arid steppe zone, Central Mongolia. *Catena* **12**, 179-
1206 190.
- 1207** Kraft, M. L., Weber, P. K., Longo, M. L., Hutcheon, I. D., and Boxer, S. G. (2006). Phase Separation of
1208 Lipid Membranes Analyzed with High-Resolution Secondary Ion Mass Spectrometry. *Science*
1209 **313**, 1948-1951.
- 1210** Krein, A., Audinot, J.-N., Migeon, H.-N., and Hoffmann, L. (2007). Facing hazardous matter in
1211 atmospheric particles with NanoSIMS. *Environmental Science and Pollution Research* **14**, 3-4.
- 1212** Kubiena, W. L. (1938). "Micropedology."
- 1213** Kuo, J., ed. (2007). "Electron Microscopy: Methods and Protocols." Humana Press, Totowa, NJ.
- 1214** Kuypers, M. M. M., and Jorgensen, B. B. (2007). The future of single-cell environmental microbiology.
1215 *Environmental Microbiology* **9**, 6-7.
- 1216** Kuzyakov, Y., Friedel, J. K., and Stahr, K. (2000). Review of mechanisms and quantification of priming
1217 effects. *Soil Biology & Biochemistry* **32**, 1485-1498.
- 1218** Lechene, C., Hillion, F., McMahon, G., Benson, D., Kleinfeld, A. M., Kampf, J. P., Distel, D., Luyten, Y.,
1219 Bonventre, J., Hentschel, D., Park, K. M., Ito, S., Schwartz, M., Benichou, G., and Slodzian, G.
1220 (2006). High-resolution quantitative imaging of mammalian and bacterial cells using stable
1221 isotope mass spectrometry. *J Biol* **5**, 20.
- 1222** Lechene, C. P., Luyten, Y., McMahon, G., and Distel, D. L. (2007). Quantitative imaging of nitrogen
1223 fixation by individual bacteria within animal cells. *Science* **317**, 1563-1566.

- 1224** Lehmann, H. (2003). Investigation of the matrix effect of Mg, Si, Ca, Sc, Fe, Y, La and Lu in pyroxene
1225 composition synthetic silicate glasses by ion microprobe. *Geostandards Newsletter-the*
1226 *Journal of Geostandards and Geoanalysis* **27**, 99-117.
- 1227** Lehmann, J., Kinyangi, J., and Solomon, D. (2007). Organic matter stabilization in soil
1228 microaggregates: implications from spatial heterogeneity of organic carbon contents and
1229 carbon forms. *Biogeochemistry* **85**, 45-57.
- 1230** Lehmann, J., Liang, B., Solomon, D., Lerotic, M., Luizao, F., Schafer, T., and Wirick, S. (2005). Near-
1231 edge x-ray absorption fine structure (NEXAFS) spectroscopy for mapping nano-scale
1232 distribution of organic carbon forms in soils: Application to black carbon particles. *Global*
1233 *Biogeochemical Cycles* **19**.
- 1234** Lehmann, J., Solomon, D., Brandes, J., Fleckenstein, H., Jacobson, C., and Thieme, J. (2009).
1235 Synchrotron-Based Near-Edge X-Ray Spectroscopy of Natural Organic Matter in Soils and
1236 Sediments. In "Biophysico-Chemical Processes Involving Natural Nonliving Organic Matter in
1237 Environmental Systems", pp. 729-781. John Wiley & Sons, Inc.
- 1238** Lemaire, R., Webb, R. I., and Yuan, Z. (2008). Micro-scale observations of the structure of aerobic
1239 microbial granules used for the treatment of nutrient-rich industrial wastewater. *ISME J* **2**,
1240 528-541.
- 1241** Li, T., Wu, T.-D., Mazéas, L., Toffin, L., Guerquin-Kern, J.-L., Leblon, G., and Bouchez, T. (2008).
1242 Simultaneous analysis of microbial identity and function using NanoSIMS. *Environmental*
1243 *Microbiology* **10**, 580-588.
- 1244** Li, Y., Dick, W. A., and Tuovinen, O. H. (2004). Fluorescence microscopy for visualization of soil
1245 microorganisms - a review. *Biology and Fertility of Soils* **39**, 301-311.
- 1246** Lombi, E., Scheckel, K. G., and Kempson, I. M. (2011). In situ analysis of metal(loid)s in plants: State of
1247 the art and artefacts. *Environmental and Experimental Botany* **72**, 3-17.
- 1248** Mangabeira, P. A., Gavrilov, K. L., de Almeida, A. A. F., Oliveira, A. H., Severo, M. I., Rosa, T. S., Silva,
1249 D. D., Labejof, L., Escaig, F., Levi-Setti, R., Mielke, M. S., Loustalot, F. G., and Galle, P. (2006).
1250 Chromium localization in plant tissues of *Lycopersicon esculentum* Mill using ICP-MS and ion
1251 microscopy (SIMS). *Applied Surface Science* **252**, 3488-3501.
- 1252** Martin, R. R., Sham, T. K., Won, G. W., Jones, K. W., and Feng, H. (2001). Synchrotron x-ray
1253 fluorescence and secondary ion mass spectrometry in tree ring microanalysis: applications to
1254 dendroanalysis. *X-Ray Spectrometry* **30**, 338-341.
- 1255** Maurice, P. A. (1996). Applications of atomic-force microscopy in environmental colloid and surface
1256 chemistry. *Colloids and Surfaces a-Physicochemical and Engineering Aspects* **107**, 57-75.
- 1257** Maurice, P. A., Lee, Y. J., and Hersman, L. E. (2000). Dissolution of Al-substituted goethites by an
1258 aerobic *Pseudomonas mendocina* var. bacteria. *Geochimica Et Cosmochimica Acta* **64**, 1363-
1259 1374.
- 1260** Messenger, S., Keller, L. P., Stadermann, F. J., Walker, R. M., and Zinner, E. (2003). Samples of stars
1261 beyond the solar system: Silicate grains in interplanetary dust. *Science* **300**, 105-108.
- 1262** Migeon, A., Audinot, J.-N., Eybe, T., Richaud, P., Damien, B., Migeon, H.-N., and Chalot, A. (2009).
1263 Cadmium and zinc localization by SIMS in leaves of *Populus deltoides* (cv. Lena) grown in a
1264 metal polluted soil. *Surface and Interface Analysis* **43**, 367-369.

- 1265** Moore, K. L., Lombi, E., Zhao, F.-J., and Grovenor, C. R. M. (2011a). Elemental imaging at the
1266 nanoscale: NanoSIMS and complementary techniques for element localisation in plants.
1267 *Analytical and Bioanalytical Chemistry* **402**, 3263-3273.
- 1268** Moore, K. L., Schroder, M., Lombi, E., Zhao, F.-J., McGrath, S. P., Hawkesford, M. J., Shewry, P. R., and
1269 Grovenor, C. R. M. (2010). NanoSIMS analysis of arsenic and selenium in cereal grain. *New*
1270 *Phytologist* **185**, 434-445.
- 1271** Moore, K. L., Schroeder, M., Wu, Z., Martin, B. G. H., Hawes, C. R., McGrath, S. P., Hawkesford, M. J.,
1272 Ma, J. F., Zhao, F.-J., and Grovenor, C. R. M. (2011b). High-Resolution Secondary Ion Mass
1273 Spectrometry Reveals the Contrasting Subcellular Distribution of Arsenic and Silicon in Rice
1274 Roots. *Plant Physiology* **156**, 913-924.
- 1275** Morales, V. L., Parlange, J. Y., and Steenhuis, T. S. (2010). Are preferential flow paths perpetuated by
1276 microbial activity in the soil matrix? A review. *Journal of Hydrology* **393**, 29-36.
- 1277** Moreau, J. W., Weber, P. K., Martin, M. C., Gilbert, B., Hutcheon, I. D., and Banfield, J. F. (2007).
1278 Extracellular proteins limit the dispersal of biogenic nanoparticles. *Science* **316**, 1600-1603.
- 1279** Mueller, C. W., Gutsch, M., Schlund, S., Prietzel, J., and Kögel-Knabner, I. (2012a). Soil aggregate
1280 destruction by ultrasonication increases soil organic matter mineralization and mobility. *Soil*
1281 *Science Society of America Journal* **76**, 1634-1643.
- 1282** Mueller, C. W., Kölbl, A., Hoeschen, C., Hillion, F., Heister, K., Herrmann, A. M., and Kögel-Knabner, I.
1283 (2012b). Submicron scale imaging of soil organic matter dynamics using NanoSIMS - From
1284 single particles to intact aggregates. *Organic Geochemistry* **42**, 1476-1488.
- 1285** Müller, B., and Defago, G. (2006). Interaction between the bacterium *Pseudomonas fluorescens* and
1286 vermiculite: Effects on chemical, mineralogical, and mechanical properties of vermiculite.
1287 *Journal of Geophysical Research-Biogeosciences* **111**.
- 1288** Musat, N., Foster, R., Vagner, T., Adam, B., and Kuypers, M. M. M. (2012). Detecting metabolic
1289 activities in single cells, with emphasis on nanoSIMS. *FEMS Microbiology Reviews* **36**, 486-
1290 511.
- 1291** Musat, N., Halm, H., Winterholler, B., Hoppe, P., Peduzzi, S., Hillion, F., Horreard, F., Amann, R.,
1292 Jørgensen, B. B., and Kuypers, M. M. M. (2008). A single-cell view on the ecophysiology of
1293 anaerobic phototrophic bacteria. *Proceedings of the National Academy of Sciences* **105**,
1294 17861-17866.
- 1295** Norton, J. M., and Firestone, M. K. (1996). N dynamics in the rhizosphere of *Pinus ponderosa*
1296 seedlings. *Soil Biology & Biochemistry* **28**, 351-362.
- 1297** Novikov, A. P., Kalmykov, S. N., Utsunomiya, S., Ewing, R. C., Horreard, F., Merkulov, A., Clark, S. B.,
1298 Tkachev, V. V., and Myasoedov, B. F. (2006). Colloid transport of plutonium in the far-field of
1299 the Mayak Production Association, Russia. *Science* **314**, 638-641.
- 1300** Nunan, N., Ritz, K., Crabb, D., Harris, K., Wu, K., Crawford, J. W., and Young, I. M. (2001).
1301 Quantification of the in situ distribution of soil bacteria by large-scale imaging of thin
1302 sections of undisturbed soil. *FEMS Microbiology Ecology* **37**, 67-77.
- 1303** Nunan, N., Young, I. M., Crawford, J. W., and Ritz, K. (2007). "Bacterial interactions at the microscale -
1304 Linking habitat to function in soil."

- 1305** Orphan, V. J., House, C. H., Hinrichs, K.-U., McKeegan, K. D., and DeLong, E. F. (2001). Methane-consuming Archaea revealed by directly coupled isotopic and phylogenetic analysis. *Science*
1306 **293**, 484-487.
1307
- 1308** Pacton, M., Ariztegui, D., Wacey, D., Kilburn, M. R., Rollion-Bard, C., Farah, R., and Vasconcelos, C.
1309 (2012). Going nano: A new step toward understanding the processes governing freshwater
1310 ooid formation. *Geology* **40**, 547-550.
- 1311** Pebesma, E. J. (2004). Multivariable geostatistics in R: the gstat package. *Computational Geoscience*
1312 **30**, 683-691.
- 1313** Peteranderl, R., and Lechene, C. (2004). Measure of carbon and nitrogen stable isotope ratios in
1314 cultured cells. *Journal of the American Society for Mass Spectrometry* **15**, 478-485.
- 1315** Pett-Ridge, J., Keiluweit, M., Zeglin, L. H., Myrold, D. D., Bougoure, J. J., Weber, P. K., Kleber, M., and
1316 Nico, P. S. (2012). Joining NanoSIMS and STXM/NEXAFS to visualize soil biotic and abiotic
1317 processes at the nano-scale. *Soil Biology and Biogeochemistry* **in review**.
- 1318** Pett-Ridge, J., and Weber, P. K. (2012). NanoSIP: NanoSIMS applications for microbial biology. *In*
1319 "Microbial Systems Biology: Methods and Protocols" (A. Navid, ed.), Vol. 881. Humana Press.
- 1320** Philippot, P., Van Zuilen, M., Lepot, K., Thomazo, C., Farquhar, J., and Van Kranendonk, M. J. (2007).
1321 Early Archaean microorganisms preferred elemental sulfur, not sulfate. *Science* **317**, 1534-
1322 1537.
- 1323** Ploug, H., Musat, N., Adam, B., Moraru, C. L., Lavik, G., Vagner, T., Bergman, B., and Kuypers, M. M.
1324 M. (2010). Carbon and nitrogen fluxes associated with the cyanobacterium *Aphanizomenon*
1325 sp. in the Baltic Sea. *ISME J* **4**, 1215-1223.
- 1326** Polerecky, L., Adam, B., Milucka, J., Musat, N., Vagner, T., and Kuypers, M. M. M. (2012).
1327 Look@NanoSIMS - a tool for the analysis of nanoSIMS data in environmental microbiology.
1328 *Environmental Microbiology* **14**, 1009-1023.
- 1329** Popa, R., Weber, P. K., Pett-Ridge, J., Finzi, J. A., Fallon, S. J., Hutcheon, I. D., Nealson, K. H., and
1330 Capone, D. G. (2007). Carbon and nitrogen fixation and metabolite exchange in and between
1331 individual cells of *Anabaena oscillarioides*. *Isme Journal* **1**, 354-360.
- 1332** Pulleman, M. M., Six, J., van Breemen, N., and Jongmans, A. G. (2005). Soil organic matter
1333 distribution and microaggregate characteristics as affected by agricultural management and
1334 earthworm activity. *European Journal of Soil Science* **56**, 453-467.
- 1335** Pumphrey, G. M., Hanson, B. T., Chandra, S., and Madsen, E. L. (2009). Dynamic secondary ion mass
1336 spectrometry imaging of microbial populations utilizing ¹³C-labelled substrates in pure
1337 culture and in soil. *Environmental Microbiology* **11**, 220-229.
- 1338** Rasmussen, B., Blake, T. S., Fletcher, I. R., and Kilburn, M. R. (2009). Evidence for microbial life in
1339 syngedimentary cavities from 2.75 Ga terrestrial environments. *Geology* **37**, 423-426.
- 1340** Remusat, L., Hatton, P.-J., Nico, P. S., Zeller, B., Kleber, M., and Derrien, D. (2012). NanoSIMS Study of
1341 Organic Matter Associated with Soil Aggregates: Advantages, Limitations, and Combination
1342 with STXM. *Environmental Science & Technology* **46**, 3943-3949.

- 1343** Rennert, T., Totsche, K. U., Heister, K., Kersten, M., and Thieme, J. (2012). Advanced spectroscopic,
1344 microscopic, and tomographic characterization techniques to study biogeochemical
1345 interfaces in soil. *Journal of Soils and Sediments* **12**, 3-23.
- 1346** Ruetting, T., Huygens, D., Staelens, J., Mueller, C., and Boeckx, P. (2011). Advances in N-15-tracing
1347 experiments: new labelling and data analysis approaches. *Biochemical Society Transactions*
1348 **39**, 279-283.
- 1349** Schaumann, G. E., and Mouvenchery, Y. K. (2012). Potential of AFM-nano thermal analysis to study
1350 the microscale thermal characteristics in soils and natural organic matter (NOM). *Journal of*
1351 *Soils and Sediments* **12**, 48-62.
- 1352** Schmidt, M. W. I., Torn, M. S., Abiven, S., Dittmar, T., Guggenberger, G., Janssens, I. A., Kleber, M.,
1353 Kogel-Knabner, I., Lehmann, J., Manning, D. A. C., Nannipieri, P., Rasse, D. P., Weiner, S., and
1354 Trumbore, S. E. (2011). Persistence of soil organic matter as an ecosystem property. *Nature*
1355 **478**, 49-56.
- 1356** Schöning, I., Morgenroth, G., and Kögel-Knabner, I. (2005). O/N-alkyl and alkyl C are stabilised in fine
1357 particle size fractions of forest soils. *Biogeochemistry* **73**, 475-497.
- 1358** Schulze, E. D., and Freibauer, A. (2005). Environmental science - Carbon unlocked from soils. *Nature*
1359 **437**, 205-206.
- 1360** Sleutel, S., Leinweber, P., Van Ranst, E., Kader, M. A., and Jegajeevagan, K. Organic Matter in Clay
1361 Density Fractions from Sandy Cropland Soils with Differing Land-Use History. *Soil Science*
1362 *Society of America Journal* **75**, 521-532.
- 1363** Slodzian, G. (1987). Basic aspects in ion imaging with secondary ions. *Scanning Microscopy*, 1-12.
- 1364** Slodzian, G., Daigne, B., Girard, F., Boust, F., and Hillion, F. (1992). Scanning secondary ion analytical
1365 microscopy with parallel detection. *Biology of the Cell* **74**, 43-50.
- 1366** Spezzano, P. (2005). Distribution of pre- and post-Chernobyl radiocaesium with particle size fractions
1367 of soils. *Journal of Environmental Radioactivity* **83**, 117-127.
- 1368** Stadermann, F. J., Walker, R. M., and Zinner, E. (1999). Nanosims: The next generation ion probe for
1369 the microanalysis of extraterrestrial material. *Meteoritics & Planetary Science* **34**, A111-A112.
- 1370** Steffens, M., Kölbl, A., Totsche, K. U., and Kögel-Knabner, I. (2008). Grazing effects on soil chemical
1371 and physical properties in a semiarid steppe of inner Mongolia (P.R. China). *Geoderma* **143**,
1372 63-72.
- 1373** Storms, H. A., Brown, K. F., and Stein, J. D. (1977). Evaluation of a cesium positive-ion source for
1374 secondary ion mass-spectrometry. *Analytical Chemistry* **49**, 2023-2030.
- 1375** Tartivel, R., Tatin, R., Delhay, T., Maupas, A., Gendron, A., Gautier, S., and Lavastre, O. (2012).
1376 Visualization and localization of bromotoluene distribution in *Hedera helix* using NanoSIMS.
1377 *Chemosphere* **89**, 805-9.
- 1378** Tippkötter, R., and Ritz, K. (1996). Evaluation of polyester, epoxy and acrylic resins for suitability in
1379 preparation of soil thin sections for in situ biological studies. *Geoderma* **69**, 31-57.

- 1380** Totsche, K. U., Rennert, T., Gerzabek, M. H., Kögel-Knabner, I., Smalla, K., Spiteller, M., and Vogel, H.
1381 J. (2010). Biogeochemical interfaces in soil: The interdisciplinary challenge for soil science.
1382 *Journal of Plant Nutrition and Soil Science* **173**, 88-99.
- 1383** Valle, N., Drillet, J., Pic, A., and Migeon, H. N. (2011). Nano-SIMS investigation of boron distribution in
1384 steels. *Surface and Interface Analysis* **43**, 573-575.
- 1385** von Lützw, M., Kögel-Knabner, I., Ekschmitt, K., Flessa, H., Guggenberg, G., Matzner, E., and
1386 Marschner, B. (2007). SOM fractionation methods: Relevance to functional pools and
1387 stabilization mechanisms. *Soil Biology & Biochemistry*.
- 1388** von Lützw, M., Kögel-Knabner, I., Ekschmitt, K., Matzner, E., Guggenberger, G., Marschner, B., and
1389 Flessa, H. (2006). Stabilization of organic matter in temperate soils: mechanisms and their
1390 relevance under different soil conditions - a review. *European Journal of Soil Science* **57**, 426-
1391 445.
- 1392** Wacey, D., Gleeson, D., and Kilburn, M. R. (2010a). Microbialite taphonomy and biogenicity: new
1393 insights from NanoSIMS. *Geobiology* **8**, 403-16.
- 1394** Wacey, D., McLoughlin, N., Whitehouse, M. J., and Kilburn, M. R. (2010b). Two coexisting sulfur
1395 metabolisms in a ca. 3400 Ma sandstone. *Geology* **38**, 1115-1118.
- 1396** Wan, J., Tyliczszak, T., and Tokunaga, T. K. (2007). Organic carbon distribution, speciation, and
1397 elemental correlations within soil microaggregates: applications of STXM and NEXAFS
1398 spectroscopy.
- 1399** Weber, K. A., Spanbauer, T. L., Wacey, D., Kilburn, M. R., Loope, D. B., and Kettler, R. M. (2012).
1400 Biosignatures link microorganisms to iron mineralization in a paleoaquifer. *Geology* **40**, 747-
1401 750.
- 1402** Weber, P., and Holt, J. (2008). "Virus and Bacterial Cell Chemical Analysis by NanoSIMS."
- 1403** Weber, P. K., Graham, G. A., Teslich, N. E., MoberlyChan, W., Ghosal, S., Leighton, T. J., and Wheeler,
1404 K. E. (2010). NanoSIMS imaging of Bacillus spores sectioned by Focused Ion Beam. *Journal of*
1405 *Microscopy* **238**, 189-199.
- 1406** Wilson, R. G., Stevie, F. A., and Magee, C. W. (1989). "Secondary Ion Mass Spectrometry: A Practical
1407 Handbook for Depth Profiling and Bulk Impurity Analysis," New York.
- 1408** Wilson, S. C., Lockwood, P. V., Ashley, P. M., and Tighe, M. (2010). The chemistry and behaviour of
1409 antimony in the soil environment with comparisons to arsenic: A critical review.
1410 *Environmental Pollution* **158**, 1169-1181.
- 1411** Wirtz, T., Fleming, Y., Gerard, M., Gysin, U., Glatzel, T., Meyer, E., Wegmann, U., Maier, U., Odriozola,
1412 A. H., and Uehli, D. (2012a). Design and performance of a combined secondary ion mass
1413 spectrometry-scanning probe microscopy instrument for high sensitivity and high-resolution
1414 elemental three-dimensional analysis. *Review of Scientific Instruments* **83**.
- 1415** Wirtz, T., Fleming, Y., Gysin, U., Glatzel, T., Wegmann, U., Meyer, E., Maier, U., and Rychen, J.
1416 (2012b). Combined SIMS-SPM instrument for high sensitivity and high-resolution elemental
1417 3D analysis. *Surface and Interface Analysis*.
- 1418** Wuebken, D., Burow, L. C., Prufert-Bebout, L., Bebout, B. M., Hoehler, T. M., Pett-Ridge, J.,
1419 Spormann, A. M., Weber, P. K., and Singer, S. W. (2012). Identification of a novel

- 1420** cyanobacterial group as active diazotrophs in a coastal microbial mat using NanoSIMS
1421 analysis. *Isme Journal* **6**, 1427-1439.
- 1422** Zimmer, D., Kruse, J., Baum, C., Borca, C., Laue, M., Hause, G., Meissner, R., and Leinweber, P. (2011).
1423 Spatial distribution of arsenic and heavy metals in willow roots from a contaminated
1424 floodplain soil measured by X-ray fluorescence spectroscopy. *Science of the Total*
1425 *Environment* **409**, 4094-4100.
- 1426**
- 1427**

Figure captions

Figure 1: A) coaxial setup of the NanoSIMS, indicating the primary and secondary ion beam in relation to the sample surface. Due to the coaxial setup, the secondary ions must have the opposite charge from the primary ions to enable extraction to the mass spectrometer. B) schematic of the NanoSIMS, with the primary ion beam in blue and the secondary ion beam in red. Courtesy of Cameca (Gennevilliers, France), adapted from Myrold et al. (2011).

Figure 2: Micrograph and microanalysis of an embedded cross section derived from a Cryosol soil core (Oa horizon, Typic Aquiturbel) from Barrow, Northern Alaska. A) back scatter electron image recorded with a SEM; B, C) NanoSIMS images ($^{12}\text{C}^{14}\text{N}^-$ and $^{56}\text{Fe}^{16}\text{O}^-$) recorded with a NanoSIMS 50 L at TU München. The back scatter SEM image shows collapsing plant cells of particulate OM in the center surrounded by mineral spheres. The red square in the SEM image indicates the area analyzed by NanoSIMS, the green line indicates the interface between particulate organic matter and mineral phase, the blue line depicts the boundary between totally and partly collapsed plant cell structures. The NanoSIMS images indicate the distribution of organic matter ($^{12}\text{C}^{14}\text{N}^-$) and the iron distribution ($^{56}\text{Fe}^{16}\text{O}^-$) within the plant cell region, and suggest organo-mineral interfaces in the early stages of formation. D) line scan data derived from analysis of NanoSIMS $^{12}\text{C}^{14}\text{N}^-$ and $^{56}\text{Fe}^{16}\text{O}^-$ secondary ion images. The line scans demonstrate the spatial distribution of both secondary ion species along a transect, illustrating the iron clusters within the organic matter region. An area of 0.5 to 0.5 μm (square #2 in images) in size was scanned along the transect (Mueller, unpublished data).

Figure 3: Back scattered secondary electron micrograph and NanoSIMS ion images ($^{16}\text{O}^-$; $^{12}\text{C}^{14}\text{N}^-$) of an embedded root tip cross-section prepared from a French oak root (*Quercus robur*, clone DF159 infected with mycorrhizal fungi *Piloderma croceum*, courtesy of F. Buscot, UFZ Halle, Germany and T. Grams, TU München, Germany) grown in a vermiculite / soil mixture. The root and adhering rhizosphere soil was fixed according to Karnovsky (1965), embedded in an epoxy resin, cross sectioned, polished and imaged via NanoSIMS. The $^{16}\text{O}^-$ NanoSIMS images illustrate thin clay mineral layers, whereas the $^{12}\text{C}^{14}\text{N}^-$ ion images

indicate the location of root cells. The row of yellow squares in the SEM image show where NanoSIMS analyses occurred, in a transect across the interfaces between root, mycorrhizal fungi and mineral particles (Mueller, unpublished data).

Figure 4: TEM and NanoSIMS images of wheat roots (*Triticum aestivum*) exposed to ^{15}N for 24 h. The samples were fixed with 2.5% glutaraldehyde in 0.1 M phosphate buffered saline and dehydrated in a graded series of acetone. The roots were infiltrated in acetone araldite mixtures over several days, using a gradually increasing araldite concentration. Final embedding in Araldite 502 was done according to Herrmann et al. (2007a). Embedded samples were cut into slices, re-embedded in 10 mm mounts and polished using silicon carbide paper and finally diamond paste. TEM images (A, D) show the presence of microorganisms in the rhizosphere (rh) and extracellular mucilage matrix (e) adjacent to the root cells (c). NanoSIMS images (B, E) of the same regions show organic matter distribution recorded as $^{12}\text{C}^{14}\text{N}$. NanoSIMS ratio images (E, F) of $^{15}\text{N}/^{14}\text{N}$ (natural abundance at 0.004), confirmed the ^{15}N enrichment of some microorganisms. Linescan data from the regions between the arrows (in C, F) is shown in G (from C) and H (from F). (Figure adapted from Clode et al. 2009) (Copyright American Society of Biologists www.plantphysiology.org).

Figure 5: SEM micrograph (Figure 1 adapted from Clode et al. 2009) of three roots (*Triticum aestivum*) in soil, showing harder materials as quartz (light areas) and softer materials including roots (dark grey areas). The loamy-sand textured soil (Ap horizon from Meckering, Western Australia) containing the roots was infiltrated in acetone araldite mixtures over several days, using a gradually increasing araldite concentration. Final embedding in Araldite 502 was done according to Herrmann et al. (2007a). Embedded samples were cut in slices, re-embedded in 10 mm mounts and polished using silicon carbide paper and finally diamond paste. (Copyright American Society of Biologists www.plantphysiology.org).

Figure 6: A soil thin section prepared by 'cryo' techniques: high pressure freezing followed by cryosectioning and then freeze drying. The soil is from a clay-rich forest soil from the H.J. Andrews Experiment Station, Oregon, USA, and was exposed in a controlled microcosm to a low-concentration ^{13}C glucose label. A) SEM micrograph collected at 2 kV; B) NanoSIMS $\delta^{13}\text{C}$ image showing what appear to be isotopically enriched microbial cells (white arrows) flanked by plant residue particles; C) STXM transmission image collected at 300 eV of the region annotated by the red/white box in (A,B), scale = 1 μm ; D) false color overlay of a STXM C difference map (ratio of scans collected above and below the C edge) and the

transmission map shown in (C); E, F) NEXAFS spectra extracted from the regions of interest circled in (D) are plotted against the standard spectra for (E) ligno-cellulose and (F) protein and substantiate plant vs. microbe particle definitions. (M. Keiluweit, J. Bougoure, P. Weber, P. Nico, M. Kleber, J. Pett-Ridge, unpublished data).

Figure 7: NanoSIMS images and semivariograms (lower panel) of an embedded cross section of organic matter derived from an aggregate of Cambisol topsoil (Ah horizon) from Höglwald, Bavaria, Germany. A) NanoSIMS $^{12}\text{C}^{14}\text{N}^-$ ion image, B) NanoSIMS $^{56}\text{Fe}^{16}\text{O}^-$ ion image. The white arrow in the NanoSIMS images indicate the line scan which was used to generate the semivariograms in C-D. (Mueller, unpublished data).

Figure 8: Microstructures associated with fungal hyphae in an organic forest soil investigated by both NanoSIMS imaging and STXM/NEXAFS spectromicroscopy. A) STXM optical density map recorded at 300 eV; B, C) NanoSIMS isotope ratio images for $^{12}\text{C}^{15}\text{N}^-/^{13}\text{C}^{14}\text{N}^-$ and Fe concentrations ($^{56}\text{Fe}^{16}\text{O}^-/^{12}\text{C}^-$, normalized to carbon) of the same feature shown in the STXM image. Brighter colors reflect high enrichment/concentration. D) Optical density map of hyphal-associated microstructures with colored regions of interest (ROIs) from which NEXAFS spectra at the C 1s absorption edge and the N 1s absorption edge were collected. ROIs are color-coded according to the spectral types extracted from them: intact fungal hyphae (grey), decomposing hyphal residue (brown), microbial residue (green) and mineral surfaces (blue). E) Average NEXAFS spectra representing the major carbon forms encountered in the regions of interest defined in D. Carbon 1s absorption edge peaks are identified as C=C 1s- π^* transition of aromatic C at 285.1 eV (a), 1s- π^* transition of C=C in ene-ketone at 286.7 eV (b), 1s-3p/ σ^* transition of aliphatic C at 287.4 eV (c), 1s- π^* transition of carboxylic and/or amide C at 288.3 eV (d), the 1s-3p/ σ^* transition of alcohol C-OH at 289.4 eV (e), and the 1s- π^* transition of carbonyl C at 290.3 eV (f). Reproduced with permission from *Geochimica and Cosmochimica Acta*.

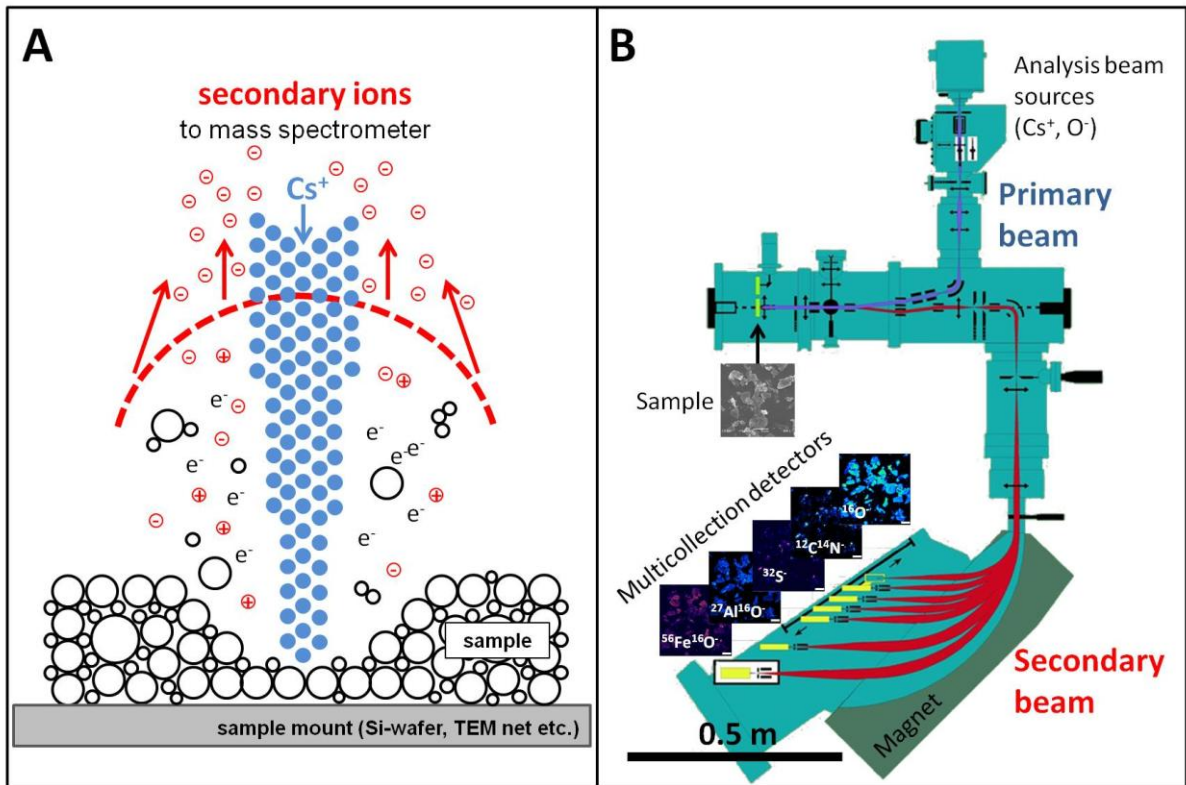


Figure 1: A) coaxial setup of the NanoSIMS, indicating the primary and secondary ion beam in relation to the sample surface. Due to the coaxial setup, the secondary ions must have the opposite charge from the primary ions to enable extraction to the mass spectrometer. B) schematic of the NanoSIMS, with the primary ion beam in blue and the secondary ion beam in red. Courtesy of Cameca (Gennevilliers, France), adapted from Myrold et al. (2011).

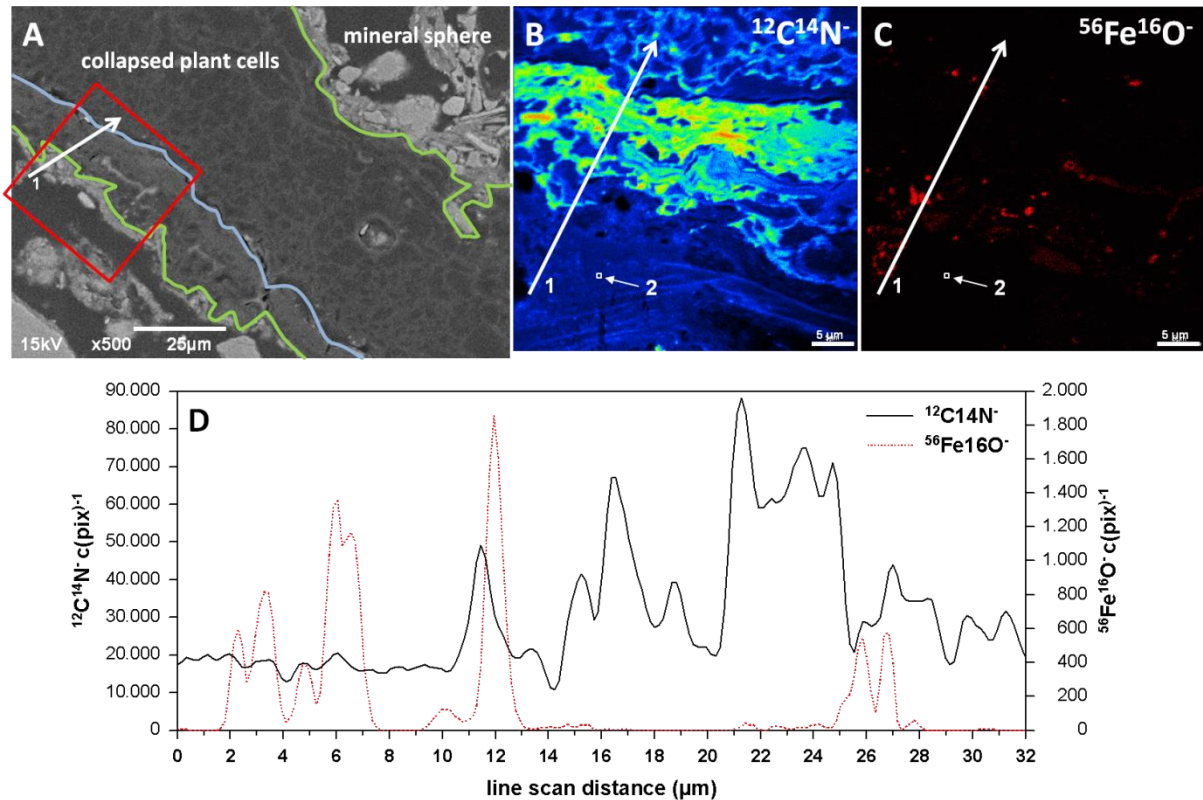


Figure 2: Micrograph and microanalysis of an embedded cross section derived from a Cryosol soil core (Oa horizon, Typic Aquiturbel) from Barrow, Northern Alaska. A) back scatter electron image recorded with a SEM; B, C) NanoSIMS images ($^{12}\text{C}^{14}\text{N}^-$ and $^{56}\text{Fe}^{16}\text{O}^-$) recorded with a NanoSIMS 50 L at TU München. The back scatter SEM image shows collapsing plant cells of particulate OM in the center surrounded by mineral spheres. The red square in the SEM image indicates the area analyzed by NanoSIMS, the green line indicates the interface between particulate organic matter and mineral phase, the blue line depicts the boundary between totally and partly collapsed plant cell structures. The NanoSIMS images indicate the distribution of organic matter ($^{12}\text{C}^{14}\text{N}^-$) and the iron distribution ($^{56}\text{Fe}^{16}\text{O}^-$) within the plant cell region, and suggest organo-mineral interfaces in the early stages of formation. D) line scan data derived from analysis of NanoSIMS $^{12}\text{C}^{14}\text{N}^-$ and $^{56}\text{Fe}^{16}\text{O}^-$ secondary ion images. The line scans demonstrate the spatial distribution of both secondary ion species along a transect, illustrating the iron clusters within the organic matter region. An area of 0.5 to 0.5 μm (square #2 in images) in size was scanned along the transect (Mueller, unpublished data).

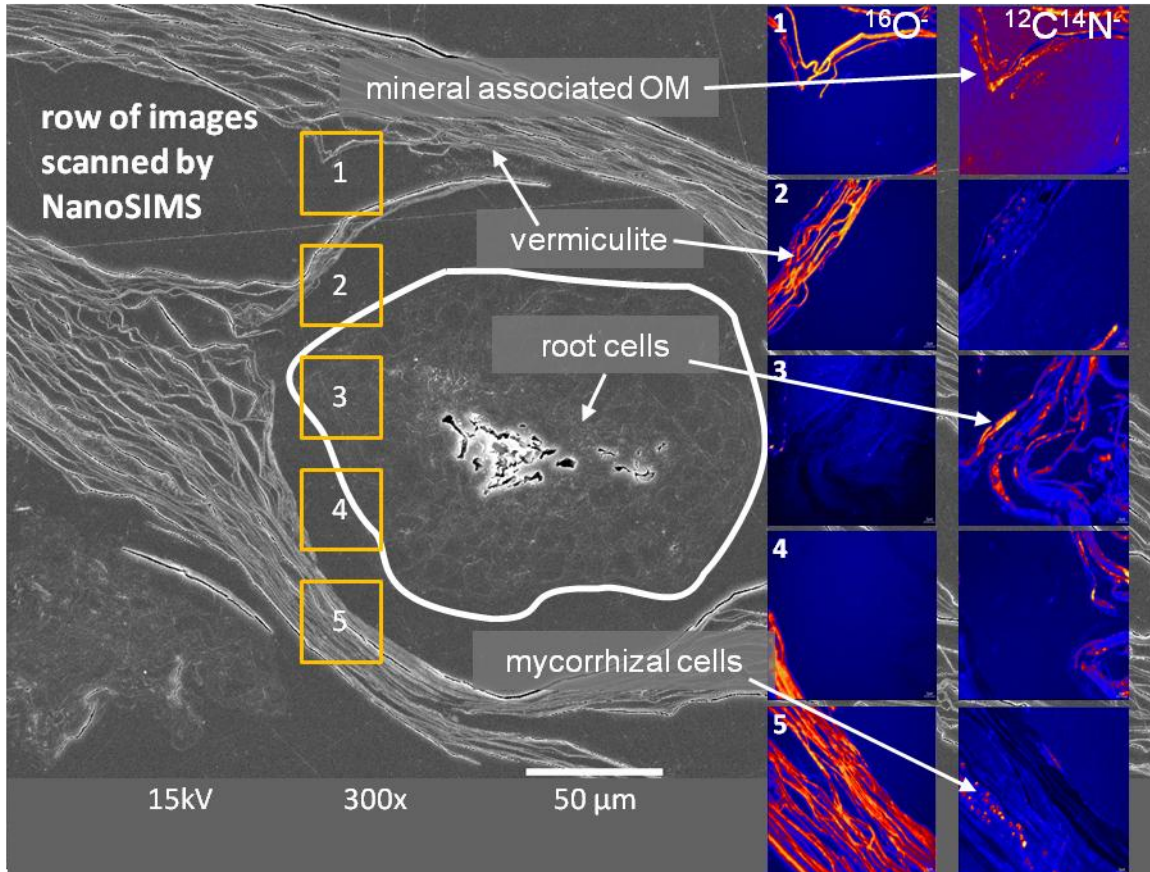


Figure 3: Back scattered secondary electron micrograph and NanoSIMS ion images ($^{16}\text{O}^-$; $^{12}\text{C}^{14}\text{N}^-$) of an embedded root tip cross-section prepared from a French oak root (*Quercus robur*, clone DF159 infected with mycorrhizal fungi *Piloderma croceum*, courtesy of F. Buscot, UFZ Halle, Germany and T. Grams, TU München, Germany) grown in a vermiculite / soil mixture. The root and adhering rhizosphere soil was fixed according to Karnovsky (1965), embedded in an epoxy resin, cross sectioned, polished and imaged via NanoSIMS. The $^{16}\text{O}^-$ NanoSIMS images illustrate thin clay mineral layers, whereas the $^{12}\text{C}^{14}\text{N}^-$ ion images indicate the location of root cells. The row of yellow squares in the SEM image show where NanoSIMS analyses occurred, in a transect across the interfaces between root, mycorrhizal fungi and mineral particles (Mueller, unpublished data).

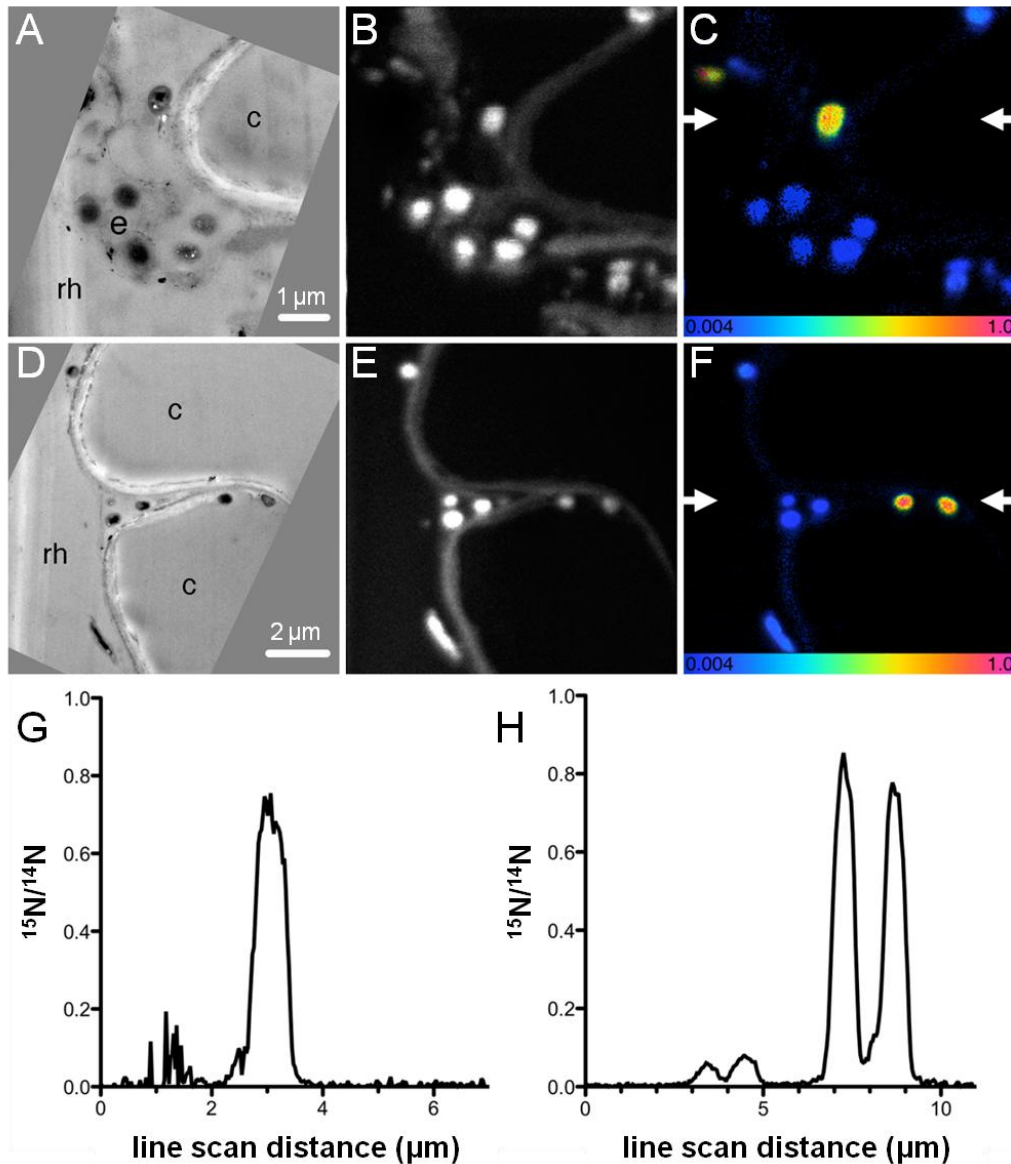


Figure 4: TEM and NanoSIMS images of wheat roots (*Triticum aestivum*) exposed to ^{15}N for 24 h. The samples were fixed with 2.5% glutaraldehyde in 0.1 M phosphate buffered saline and dehydrated in a graded series of acetone. The roots were infiltrated in acetone araldite mixtures over several days, using a gradually increasing araldite concentration. Final embedding in Araldite 502 was done according to Herrmann et al. (2007a). Embedded samples were cut into slices, re-embedded in 10 mm mounts and polished using silicon carbide paper and finally diamond paste. TEM images (A, D) show the presence of microorganisms in the rhizosphere (rh) and extracellular mucilage matrix (e) adjacent to the root cells (c). NanoSIMS images (B, E) of the same regions show organic matter distribution recorded as $^{12}\text{C}^{14}\text{N}$. NanoSIMS ratio images (E, F) of $^{15}\text{N}/^{14}\text{N}$ (natural abundance at 0.004), confirmed the ^{15}N enrichment of some microorganisms. Linescan data from the regions between the arrows (in C, F) is shown in G (from C) and H (from F). (Figure adapted from Clode et al. 2009) (Copyright American Society of Biologists www.plantphysiology.org).

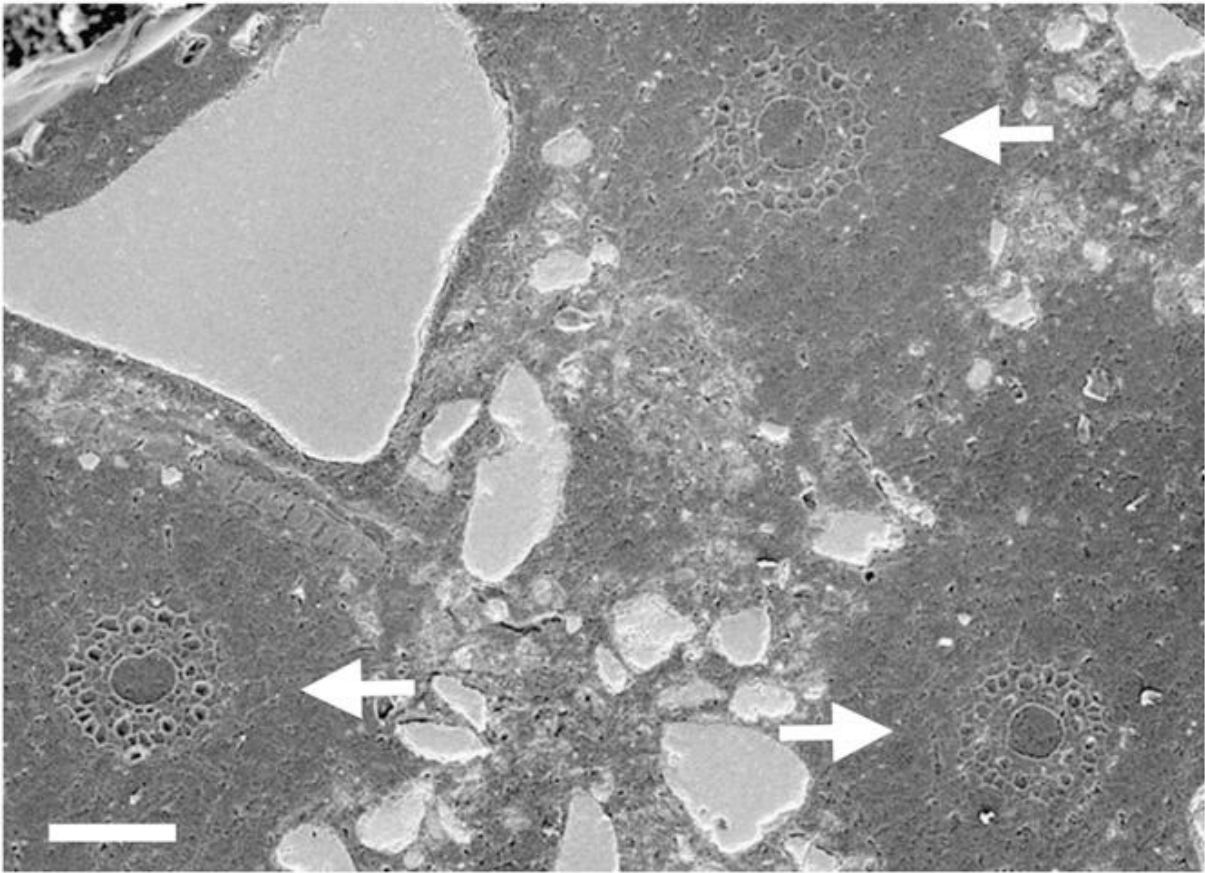


Figure 5: SEM micrograph (Figure 1 adapted from Clode et al. 2009) of three roots (*Triticum aestivum*) in soil, showing harder materials as quartz (light areas) and softer materials including roots (dark grey areas). The loamy-sand textured soil (Ap horizon from Meckering, Western Australia) containing the roots was infiltrated in acetone araldite mixtures over several days, using a gradually increasing araldite concentration. Final embedding in Araldite 502 was done according to Herrmann et al. (2007a). Embedded samples were cut in slices, re-embedded in 10 mm mounts and polished using silicon carbide paper and finally diamond paste. (Copyright American Society of Biologists www.plantphysiology.org).

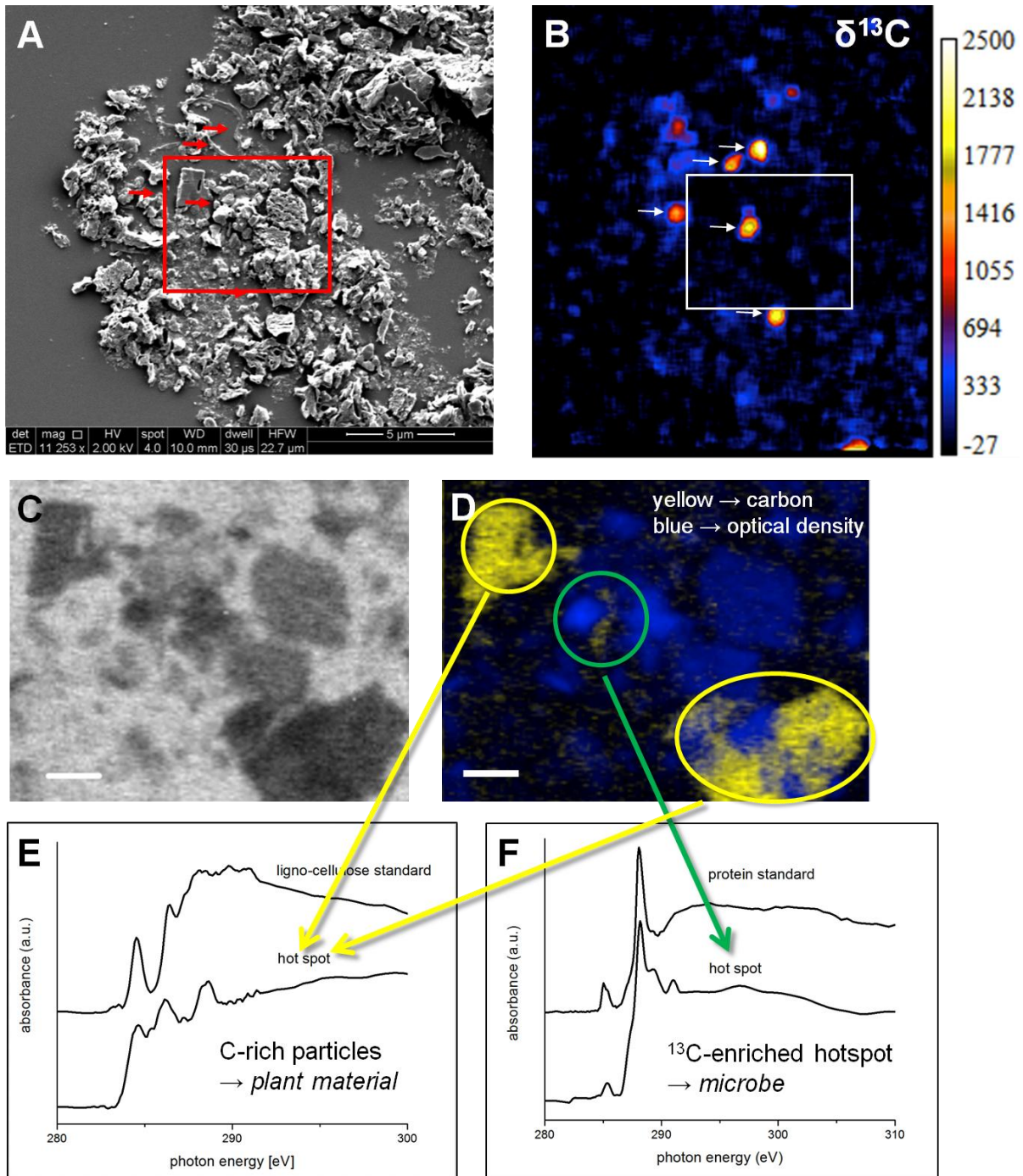


Figure 6: A soil thin section prepared by ‘cryo’ techniques: high pressure freezing followed by cryosectioning and then freeze drying. The soil is from a clay-rich forest soil from the H.J. Andrews Experiment Station, Oregon, USA, and was exposed in a controlled microcosm to a low-concentration ^{13}C glucose label. A) SEM micrograph collected at 2 kV; B) NanoSIMS $\delta^{13}\text{C}$ image showing what appear to be isotopically enriched microbial cells (white arrows) flanked by plant residue particles; C) STXM transmission image collected at 300 eV of the region annotated by the red/white box in (A,B), scale = 1 μm ; D) false color overlay of a

STXM C difference map (ratio of scans collected above and below the C edge) and the transmission map shown in (C); E, F) NEXAFS spectra extracted from the regions of interest circled in (D) are plotted against the standard spectra for (E) ligno-cellulose and (F) protein and substantiate plant vs. microbe particle definitions. (M. Keiluweit, J. Bougoure, P. Weber, P. Nico, M. Kleber, J. Pett-Ridge, unpublished data).

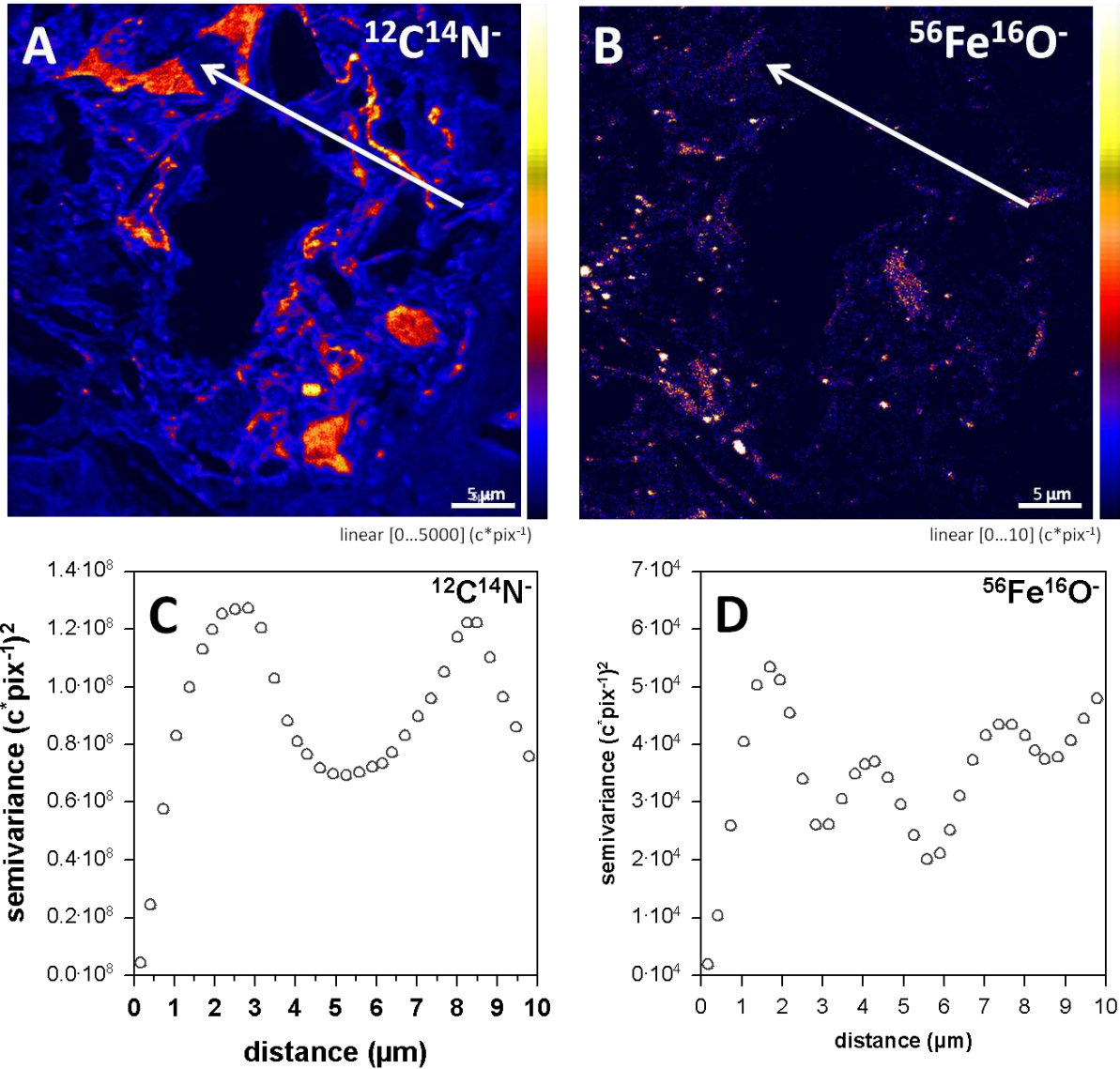


Figure 7: NanoSIMS images and semivariograms (lower panel) of an embedded cross section of organic matter derived from a aggregate of Cambisol topsoil (Ah horizon) from Höglwald, Bavaria, Germany. A) NanoSIMS $^{12}\text{C}^{14}\text{N}^-$ ion image, B) NanoSIMS $^{56}\text{Fe}^{16}\text{O}^-$ ion image. The white arrow in the NanoSIMS images indicate the line scan which was used to generate the semivariograms in C-D. (Mueller, unpublished data).

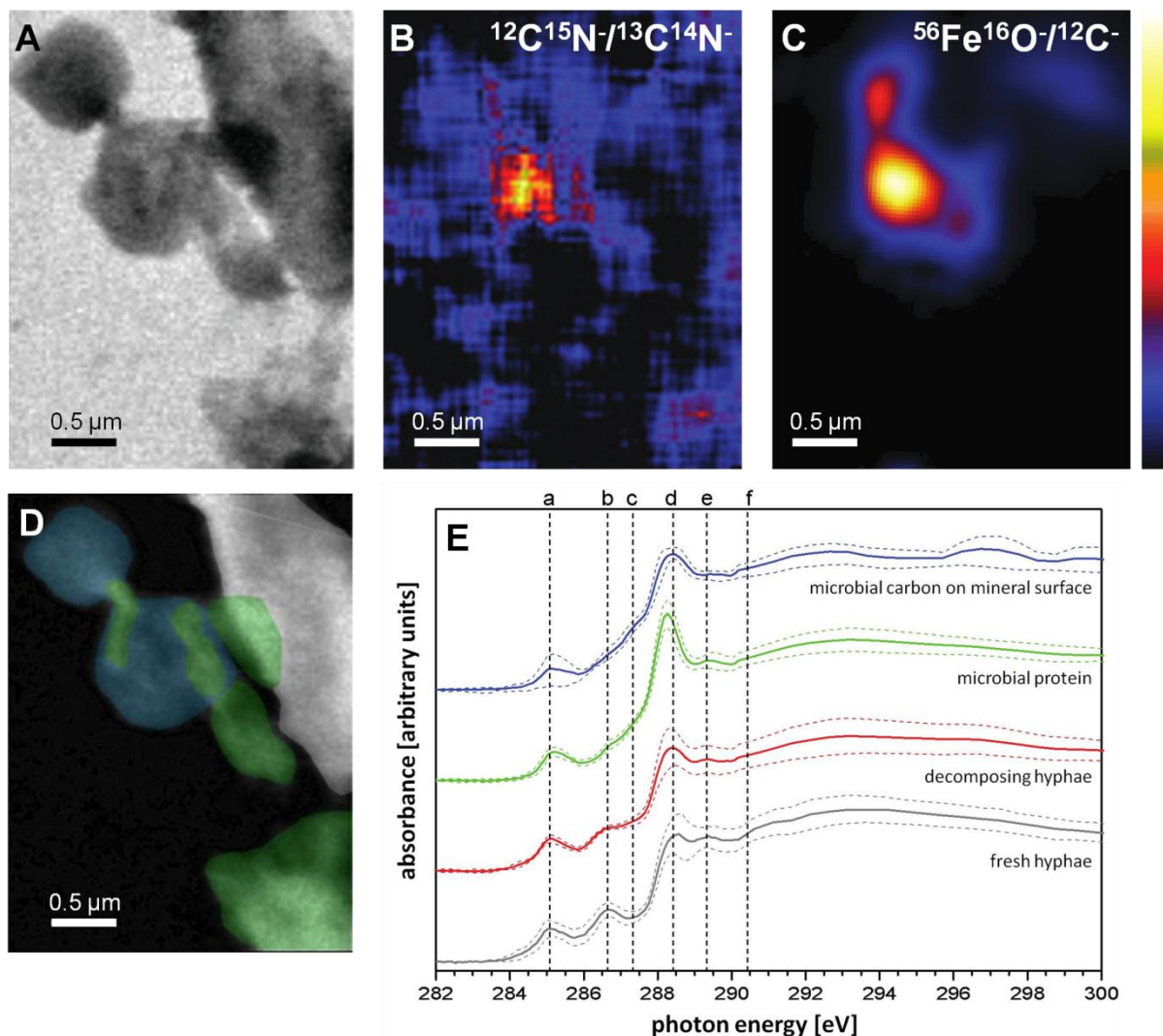


Figure 8: Microstructures associated with fungal hyphae in an organic forest soil investigated by both NanoSIMS imaging and STXM/NEXAFS spectromicroscopy. A) STXM optical density map recorded at 300 eV; B, C) NanoSIMS isotope ratio images for $^{12}\text{C}^{15}\text{N}/^{13}\text{C}^{14}\text{N}$ and Fe concentrations ($^{56}\text{Fe}^{16}\text{O}/^{12}\text{C}$, normalized to carbon) of the same feature shown in the STXM image. Brighter colors reflect high enrichment/concentration. D) Optical density map of hyphal-associated microstructures with colored regions of interest (ROIs) from which NEXAFS spectra at the C 1s absorption edge and the N 1s absorption edge were collected. ROIs are color-coded according to the spectral types extracted from them: intact fungal hyphae (grey), decomposing hyphal residue (brown), microbial residue (green) and mineral surfaces (blue). E) Average NEXAFS spectra representing the major carbon forms encountered in the regions of interest defined in D. Carbon 1s absorption edge peaks are identified as C=C 1s- π^* transition of aromatic C at 285.1 eV (a), 1s- π^* transition of C=C in ene-ketone at 286.7 eV (b), 1s-3p/ σ^* transition of aliphatic C at 287.4 eV (c), 1s- π^* transition of carboxylic and/or amide C at 288.3 eV (d), the 1s-3p/ σ^* transition of alcohol C-OH at 289.4

eV (e), and the $1s-\pi^*$ transition of carbonyl C at 290.3 eV (f). Reproduced with permission from *Geochimica and Cosmochimica Acta*.